Continental Shelf Research 249 (2022) 104855

Contents lists available at ScienceDirect

Continental Shelf Research

journal homepage: www.elsevier.com/locate/csr

Research papers

Seasonal nutrient co-limitation in a temperate shelf sea: A modelling approach

Angela A. Bahamondes Dominguez [a,*], Helen S. Macdonald [a], Graham Rickard [a], Matthew L. Hammond [b]

[a] National Institute of Water and Atmospheric Research, Evans Bay Parade, Hataitai, Wellington 6021, New Zealand
[b] National Oceanography Centre, European Way, Southampton SO14 3ZH, United Kingdom

ARTICLE INFO

Keywords:
Shelf sea biogeochemistry
Biogeochemical modelling
Celtic sea
Dissolved iron
Nitrate
Primary production

ABSTRACT

Nutrient limitation on phytoplankton growth plays a critical role in ocean productivity, the functioning of marine ecosystems, and the ocean carbon cycle. In the Celtic Sea, a temperate shelf sea, many studies have shown the importance of nitrate on phytoplankton growth focusing on the seasonal cycle of nitrate and feedbacks with the physical environment; but only recently has it been demonstrated, through discrete measurements, that dissolved iron also plays an important role in the ecosystem of the region. A well-established one-dimensional model has been developed to analyse the nutrient co-limitation between dissolved iron and dissolved inorganic nitrogen in the Celtic Sea. This model allows us to study the full seasonal cycle and inter-annual variability of these two nutrients. Simulations show that dissolved iron is an important nutrient for the development of the spring bloom, while nitrate plays a more important role during the summer season. Sensitivity analyses show that these results are robust when varying the nutrient-related parameters; the largest variability observed for primary production was observed when varying the nutrient sediment flux rates for dissolved iron and nitrate while less impact on phytoplankton production occurs when changing the half saturation constants. Here, we demonstrate that dissolved iron is an important nutrient for the development of the spring bloom and it should not be neglected as a state variable when modelling the Celtic Sea or other temperate shelf seas.

1. Introduction

Shelf seas play an important role in the biological carbon pump, a set of processes by which CO_2 from the atmosphere is fixed into organic matter via photosynthesis and sequestered into the deep ocean, as they are responsible for 15 to 30% of the global oceanic primary production (PP) (Wollast, 1998; Muller-Karger et al., 2005; Davis et al., 2014). Due to their exceptionally high biological productivity (Holt and Proctor, 2008), it is important to understand the drivers of PP in shelf seas. This study is focused in the Celtic Sea, a temperate shelf sea that forms part of the northwest European continental shelf. As part of the U.K. Shelf Sea Biogeochemistry programme (http://www.uk-ssb.org/), a series of sampling campaigns were conducted at the Central Celtic Sea (CCS) location, providing a good opportunity to determine the key controls on the magnitude of PP exerted by light, grazing pressure, and nutrient availability.

Due to the seasonal stratification in the Celtic Sea, vertical mixing determines the availability of light and nutrients to phytoplankton (Sverdrup, 1953; Pingree and Pennycuick, 1975; Pingree et al., 1976). Seasonal stratification usually occurs in April and, as phytoplankton gets trapped in the euphotic zone, a spring bloom forms (Pingree et al., 1976; Fasham et al., 1983). During this period of time, nitrate (NO_3) is exhausted (<0.02 mmol N m^{-3}) in the surface mixed layer (SML) but increases below the thermocline due to regeneration of organic material (Pingree et al., 1977; Sharples et al., 2001; Rippeth et al., 2009; Hickman et al., 2009, 2012). This complete drawdown of NO_3 suggests that this nutrient is a limiting factor for PP (Sharples et al., 2001; Williams et al., 2013a,b). Great importance has been given to the seasonal cycle of nitrate in the Celtic Sea. Other studies have focused on the seasonal cycle of silica and phosphorus, showing that silica is a limiting nutrient for the spring diatom growth (Poulton et al., 2019b) but observations show that diatoms only contribute, on average, a small percentage in average to the net primary production (NPP) of the CCS location; while Poulton et al. (2019a) showed low phosphorus concentrations and depleted nitrate during summer. However, Birchill et al. (2017) demonstrated that NO_3 is not the only important limiting nutrient in the Celtic Sea and that dissolved iron (dFe) also plays a

* Corresponding author.
E-mail address: angela.bahamondesdominguez@niwa.co.nz (A.A. Bahamondes Dominguez).

https://doi.org/10.1016/j.csr.2022.104855
Received 8 February 2022; Received in revised form 15 September 2022; Accepted 20 September 2022
Available online 29 September 2022

crucial role, creating an environment for phytoplankton growth that is co-limited by dFe and NO_3.

Iron (Fe) is an essential micronutrient for marine primary producers, limiting their growth in large parts of the world's ocean (Boyd and Ellwood, 2010). It has been observed that Fe limitation usually occurs in high-nitrate, low-chlorophyll (HNLC) regions (Boyd et al., 2007), but Fe has also been reported as a limiting nutrient in coastal regions and shelf seas (Hutchins and Bruland, 1998; Birchill et al., 2017). Moreover, as phytoplankton play a significant role in CO_2 uptake from the atmosphere, Fe is argued to be important in the regulation of the global climate (Sigman and Boyle, 2000). Therefore, it is important to understand the sources of Fe and how it is cycled and removed from the ocean. Shelf seas are assumed to be Fe replete due to riverine and groundwater inputs, sediment resuspension, and diagenetic supplies (Elrod et al., 2004; Chase et al., 2005; Ussher et al., 2007; Lohan and Bruland, 2008; Homoky et al., 2012; Birchill et al., 2017). For the Celtic Sea, a shallow shelf sea (with depths up to 200 m; Sharples et al. (2013)), with deep mixing being observed during winter and stratification during summer (Williams et al., 2013b), sediments underlying the shelf have been argued to be a major source of Fe (Johnson et al., 1999; Elrod et al., 2004; Severmann et al., 2010; Homoky et al., 2012; Conway and John, 2014; Dale et al., 2015).

Nutrients limiting phytoplankton growth in the ocean are a critical control on ocean productivity (Browning et al., 2022). Recent research have provided insights into the importance of nutrient co-limitation by two or more nutrients, suggesting that in the modern ocean there is no single nutrient that could be considered limiting in isolation (Moore et al., 2013). For example, Bonnet et al. (2008)'s study found that in the South Pacific gyre primary productivity is Fe and N co-limited. Similarly, Moisander et al. (2012) suggested a co-limitation between phosphate and dissolved iron for N_2 fixation for diazotrophs in the South Pacific (from Australia to Fiji). Moore et al. (2008) conducted nutrient addition bioassay experiments in the subtropical North Atlantic Ocean to investigate the influence of nitrogen, phosphorus, and dissolved iron on limiting PP finding a phosphorus/nitrate co-limitation for the growth of *Synechococcus*. Furthermore, nutrient co-limitation has also been observed in the Subantarctic Southern Ocean (Sedwick et al., 2002), where experimental results revealed that phytoplankton growth is primarily limited by macronutrients (nitrate and phosphate) but iron deficiency imposed a significant secondary limitation on community growth.

The majority of large-scale numerical ocean biogeochemical models assume phytoplankton growth to be proportional to the external nutrient concentration assuming a Monod type model, with nutrient uptake parameterised as a saturating function of external nutrient concentrations using a Michaelis–Menten functional form (Moore et al., 2001a; Flynn, 2010; Steinacher et al., 2010). Co-limitation by different nutrients is then usually conformed to the minimum-type concept where growth is dictated by the smallest value of the Michaelis–Menten terms. Many of these models also assume a constant stoichiometry, however, nutrient limitation have been shown to be linked to intracellular stoichiometric variability (see Moore et al. (2013) for more information).

Here, we use a 1-D model to understand the importance of co-limitation between dFe and dissolved inorganic nitrogen (DIN) in the Celtic Sea for phytoplankton growth and PP. Due to their low computational cost, 1-D models are a useful tool to run a large number of experiments and sensitivity analyses. One-dimensional models have been widely used in the literature to understand different processes of marine biogeochemistry in a range of locations such as the Ross Sea (Worthen and Arrigo, 2003; Kaufman et al., 2017), Amundsen Sea (Oliver et al., 2019), subarctic Pacific Ocean (Denman and Peña, 1999), Southern Ocean (Hannon et al., 2001), Baltic Sea (Fennel, 1995), amongst many others. For this research, a more recent version of the Shelf Sea Physics and Primary Production (S2P3) model (Sharples, 1999; Simpson and Sharples, 2012) known as S2P3 v8.0 (Bahamondes Dominguez et al., 2020) has been developed to introduce dFe as a co-limiting nutrient. This well established 1-D model exploits the dominance of vertical processes over horizontal processes in shelf seas and has been used to simulate idealised seasonal tidal mixing fronts (Sharples, 2008), to analyse the timing of the spring bloom in the North Sea (Sharples et al., 2006), and to study different regional configurations (e.g. northwest European shelf, English Channel, and the East China and Yellow Seas; Marsh et al. (2015)). Furthermore, a variable stoichiometry is considered in the S2P3 v8.0 model for phytoplankton photo-acclimation (Bahamondes Dominguez et al., 2020). For this work, a thorough analysis in terms of sensitivity to nutrient sources, concentrations, and assimilation provides details on the responses of phytoplankton growth, giving a more fully seasonal and inter-annual representation of nutrient co-limitation validated by discrete observations of dFe and DIN from the work of Birchill et al. (2017).

2. Methods

2.1. Model setup and development

This 1-D model allows a representation of the water column in terms of the physical and biological processes in shelf seas; it can simulate the seasonal cycle of phytoplankton, water column stratification, and PP. The physical model has been described in detail in many other studies (Sharples, 1999; Sharples et al., 2006; Sharples, 2008; Simpson and Sharples, 2012; Marsh et al., 2015). This model is developed here to include a more complex representation of the ecosystem based on the S2P3 v8.0 model (Bahamondes Dominguez et al., 2020).

This study is focused on the Central Celtic Sea (CCS; $49.4°N$, $8.6°W$), a shallow region (140 m depth) located in the North-Western (NW) European Shelf (Fig. 1a), which is characterised by its tidally dynamic environment and summer stratification (Pingree et al., 1978; Sharples and Holligan, 2006; Hickman et al., 2012). Daily meteorological data from the National Centers for Environmental Predictions (NCEP) Reanalysis data (http://www.esrl.noaa.gov/psd) are used to force the model, including wind speed (m s^{-1}), cloud coverage (%), air temperature (°C), and relative humidity (%) variables. The model also has an input from tides predicted by the Proudman Oceanographic Laboratory Coastal Ocean Modelling Systems (POLCOMS) 3-D shelf model (Holt et al., 2009; Wakelin et al., 2009), including the three main tidal constituents for the CCS location: M_2, S_2, and N_2, providing a persistent background level of mixing. This model considers a turbulence closure scheme for which the prognostic variable is the turbulent kinetic energy (TKE); in S2P3 v8.0, tides and winds force the TKE profile through surface (winds) and near-bottom (tides) boundary conditions (for more information see Marsh et al. (2015)). The spring–neap cycle of stronger mixing (on spring tides) and strengthened stratification (on neap tides) causes variations in the Chl-a concentration in a 14-day cycle (Sharples, 1999; Sharples et al., 2006; Marsh et al., 2015).

S2P3 v8.0 resolves 8 state variables distributed between nitrogen and dissolved iron cycles, considering nitrogen as the main currency of this model. The remaining state variables denote one species of phytoplankton in nitrogen, chlorophyll, iron, and carbon currencies; and two other pools for zooplankton and detritus (or DOM; Fig. 1b). In this framework, a variable elemental ratio is allowed based on the work by Geider et al. (1998), which includes stoichiometry changes for C : N : Chl allowing us to estimate the cycle of carbon. The stoichiometric ratios are defined as: $Q = N : Chl$, $Q_P = N : C$, $\theta = Chl : C$, and $Q_{Fe} = Fe : N$. For simplicity, there is a fixed ratio for N : Fe, making dissolved iron to be rigidly coupled to nitrogen, so there is no state variable for detrital iron. Note that this model considers DIN to represent all forms of nitrogen: nitrate, nitrite (NO_2), and ammonium (NH_4). All parameters from the following equations are specified in Table 1.

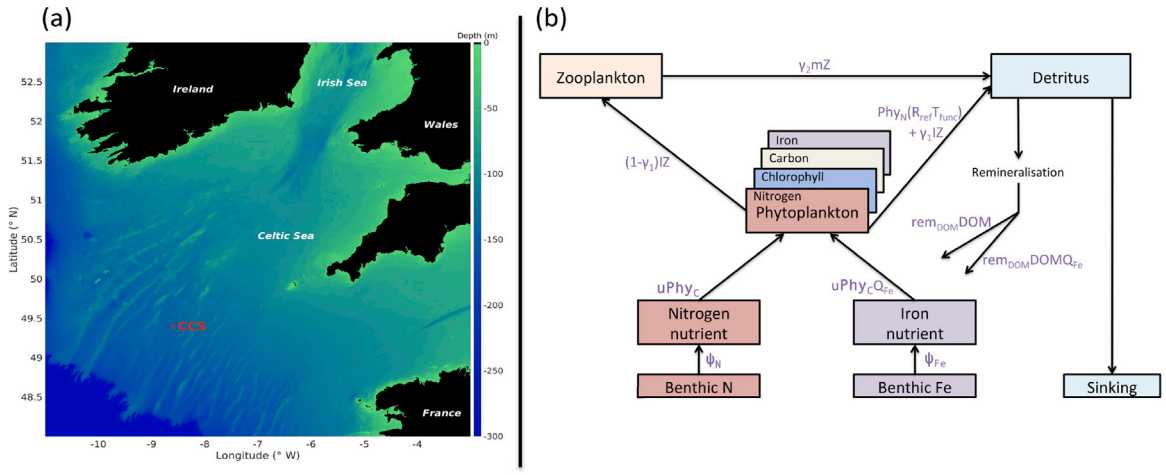

Fig. 1. (a) Map of the study area for the CCS location (in red colour). Image created with Matlab using the repository data for gridded bathymetry provided by General Bathymetric Chart of the Oceans (GEBCO). (b) Schematic diagram of the components and interactions in the S2P3 v8.0 model. Overlapping boxes indicate components for a state variable with multiple currencies modelled.

Phytoplankton growth is calculated as a parameterisation to changes in light, nutrients, and temperature as:

$$\mu = P_m(1 - e^{-\left(\frac{\alpha^{chl} I_{PAR} \theta}{P_m}\right)}), \tag{1}$$

where I_{PAR} is the photosynthetically available radiation.

The carbon-specific, light-saturated photosynthetic rate (Moore et al., 2001b) is calculated as:

$$P_m = P^C_{max} f. \tag{2}$$

The carbon-specific, light-saturated photosynthetic rate depends on the internal nitrogen status of the cells. Following the approach of Geider et al. (1998) and Moore et al. (2001b), where P_m provides a significant link between carbon metabolism and the nitrogen nutritional state of the phytoplankton. f allows for a variable C:N ratio, where Q is constrained to be $\geq Q_{min}$ and $\leq Q_{max}$, given by:

$$f = \frac{Q - Q_{min}}{Q_m - Q_{min}}. \tag{3}$$

Nutrient limitation of phytoplankton growth is calculated via the standard, hyperbolic Michaelis–Menten equation (Eq. (4)), using ambient nutrient concentrations and parameters for the concentration at which phytoplankton growth is half its theoretical maximum (half-saturation constants K_{Fe} and K_N Geider et al., 1998; Moore et al., 2001b). The approach used in this work for nutrient co-limitation is widely used in the literature for modelling studies that consider multiple pools of macro- and micro-nutrients (Moore et al., 2001b; Fiechter et al., 2009; Aumont et al., 2015). Nutrient assimilation is given by:

$$u = u_m \left(\frac{1 - f}{1.015 - f}\right) * min\left(\frac{N}{K_N + N}, \frac{Fe}{K_{Fe} + Fe}\right). \tag{4}$$

The minimum values given by the nutrient concentration and their half-saturation constant defined as N_{lim} for DIN and Fe_{lim} for dFe varies over the year and can estimate which nutrient is the one limiting phytoplankton growth. The rate of change for these variables ranges between 0 to 1 and they are dimensionless, so they provide an easy proxy to study nutrient co-limitation.

$$Nlim = \frac{N}{K_N + N}, \tag{5}$$

$$Fe_{lim} = \frac{Fe}{K_{Fe} + Fe}. \tag{6}$$

The model explicitly simulates carbon (Phy_C; mg C m^{-3}), iron (Phy_{Fe}; μmol Fe m^{-3}), nitrate (Phy_N; mmol N m^{-3}), and chlorophyll (Phy_{Chl}; mg Chl-a m^{-3}) for the phytoplankton pool, but the main currency of this model is in nitrogen (N). The full model phytoplankton equations are given by:

$$\frac{\partial Phy_C}{\partial t} = \frac{\partial}{\partial z}\left(K_Z \frac{\partial Phy_C}{\partial z}\right) + Phy_C(\mu - R_{ref} T_{func} - u\zeta) - I\frac{Z}{Q_P}, \tag{7}$$

$$\frac{\partial Phy_{Fe}}{\partial t} = \frac{\partial}{\partial z}\left(K_Z \frac{\partial Phy_{Fe}}{\partial z}\right) + uPhy_C Q_{Fe} - Phy_{Fe}(R_{ref} T_{func}) - IZQ_{Fe}, \tag{8}$$

$$\frac{\partial Phy_N}{\partial t} = \frac{\partial}{\partial z}\left(K_Z \frac{\partial Phy_N}{\partial z}\right) + uPhy_C - Phy_N(R_{ref} T_{func}) - IZ, \tag{9}$$

$$\frac{\partial Phy_{chl}}{\partial t} = \frac{\partial}{\partial z}\left(K_Z \frac{\partial Phy_{chl}}{\partial z}\right) + u\rho_{chl} Phy_C - Phy_{chl}(R_{ref} T_{func}) - I\frac{Z}{Q}, \tag{10}$$

where K_Z is a depth-, time-dependent coefficient of vertical eddy diffusivity; the losses for phytoplankton are due to grazing and respiration ($R_{ref} T_{func}$; where T_{func} is a temperature-response function of phytoplankton), and the cost of biosynthesis ζ.

The chlorophyll-a synthesis is calculated as:

$$\rho_{chl} = \theta^N_{max}\left(\frac{\mu}{\alpha^{chl} I_{PAR} \theta}\right). \tag{11}$$

Zooplankton grazing on phytoplankton response depends on a Holling type 2 or Ivlev grazing (Franks, 2002), with the ingestion rate of zooplankton (I) defined as:

$$I = R_m(1 - e^{(-\lambda Phy_N)}). \tag{12}$$

Zooplankton predation on phytoplankton depends on phytoplankton biomass and their ability to predate. Zooplankton biomass is calculated as:

$$\frac{\partial Z}{\partial t} = \frac{\partial}{\partial z}\left(K_Z \frac{\partial Z}{\partial z}\right) + (1 - \gamma_1) IZ - mZ. \tag{13}$$

The detrital pool or dissolved organic matter (DOM) consists of phytoplankton respiration (Phy_N*R_{ref}), sloppy feeding or zooplankton messy eating (γ_1*I*Z), and dead zooplankton (γ_2*m*Z). In the ocean, attached bacteria can break down the detritus into utilisable nutrient, a process known as remineralisation. This model does not explicitly model bacteria but it represents detrital remineralisation as rem_{DOM}*DOM. Detrital particles can aggregate together and sink out of the mixed layer, a mechanism that plays an important part in exporting carbon to the deep

ocean (Edwards, 2001). This model calculates a sinking loss term for detritus as $w_{DOM} * \partial DOM/\partial z$. The DOM pool in the model is given by:

$$\frac{\partial DOM}{\partial t} = \frac{\partial}{\partial z}\left(K_Z \frac{\partial DOM}{\partial z}\right) + \gamma_1 IZ + \gamma_2\, mZ + Phy_N(R_{ref}T_{func}) - rem_{DOM}\, DOM - w_{DOM}\frac{\partial DOM}{\partial z}. \quad (14)$$

Finally, the changes in time for DIN and dFe are calculated based on the gains through a fraction of remineralised detrital material while the main loss for the nutrient pools is given by the uptake or nutrient assimilation by phytoplankton. DIN is calculated as:

$$\frac{\partial N}{\partial t} = \frac{\partial}{\partial z}\left(K_Z \frac{\partial N}{\partial z}\right) + rem_{DOM}\, DOM - uPhy_C. \quad (15)$$

The dissolved iron pool is given by:

$$\frac{\partial Fe}{\partial t} = \frac{\partial}{\partial z}\left(K_Z \frac{\partial Fe}{\partial z}\right) + rem_{DOM}\, DOM Q_{Fe} - uPhy_C Q_{Fe}. \quad (16)$$

Nutrients are also supplied by resuspension at the seabed, with a boundary condition applied to the bottom depth cell of the model grid following Sharples (1999)'s approach:

$$\psi_N = N_{rate}\left(\frac{N_{sed} - N_0}{N_{sed}}\right), \quad (17)$$

$$\psi_{Fe} = Fe_{rate}\left(\frac{Fe_{sed} - Fe_0}{Fe_{sed}}\right), \quad (18)$$

where N_{rate} and Fe_{rate} (d^{-1}) are an input rate parameters for DIN and dFe, respectively. The parameters N_{sed} and Fe_{sed} are an assumed maximum value for near bed DIN and dFe; N_0 and Fe_0 are variables representing the bottom depth cell nutrient concentration for DIN and dFe, respectively. Application of Eqs. (17) and (18) determine the rate of DIN and dFe replenishment throughout the water column once vertical homogeneity is achieved after the autumnal equinox.

2.2. Sensitivity analysis

A percentage of time-depth points where the system is nitrate limited was calculated as:

$$N_{lim}^{perc} = \sum_{t=1}^{n}\sum_{l=1}^{N}((Fe_{lim} > N_{lim})/(n * N)) * 100, \quad (19)$$

where n is the maximum number of days of simulation (t) and N is the maximum number of vertical levels (l) in the model (equal to 140).

2.3. Model calibration and validation: UK SSB programme

The model is initialised on 1st January of the first year of simulation (year 1960) with a temperature of 10.10 °C at all depths (based on buoy observations for winter), with the water column presumed mixed throughout. The first five years of simulation are considered as model spin-up and are not analysed. The vertical resolution in this work is 1 m (i.e. 140 vertical levels).

Initial values of physical variables are consistent with former studies (Sharples, 1999, 2008; Marsh et al., 2015), whereas the initial values of the following biological variables are: zooplankton biomass, 0.02 mmol N m^{-3} (Giering et al., 2018); phytoplankton chlorophyll, 0.2 mg Chl m^{-3} (Mills et al., 2003), and the DIN initial value is 7 mmol N m^{-3} (from observed CTD data). CTD casts were collected at the CCS location, with discrete samples of nitrate plus nitrite. According to these observations and the work of Alridge et al. (2017), nitrate is the dominant form of DIN in the CCS location in comparison to nitrite and ammonium. The CTD samples were collected from pre-dawn to midday with a 1 m vertical resolution over the whole water column. This data allowed us to set an initial condition of modelled dFe of 1.85 (μmol Fe m^{-3}), which is the mean value observed for dFe at the bottom layers of the water column during November 2014. The initialised variables are only set up at the start of each simulation and do not reset between years.

To calibrate the newly developed model, *in situ* observations were used from the UK SSB programme. We use a trial-and-error approach informed by literature values to perform an exhaustive comparison between each provided observation for the CCS location and the model. For this comparison, we focused on the available observations from Birchill et al. (2017) to estimate the value of dFe at the bottom of the water column and to find the closest match to the vertical profiles of dFe data. Other model parameters were calibrated based on the work of Bahamondes Dominguez et al. (2020) that considered DIN observations; Moore et al. (2006)'s observations for physiological parameters; Giering et al. (2018)'s work for zooplankton biomass; and Edwards (2001)'s estimations of DOM remineralisation and sinking rates. The remaining parameters for which there were no observations available for the CCS location (e.g., K_N, K_{Fe}, R_m, etc.) were calibrated against all observations available, requiring hundreds of experiments to be run in order to match the model with the data. A range of values for these parameters was taken into account for the ones that could be found in the literature; estimates from models and other studies for K_N suggest a range of [0.1–2.5] mmol N m^{-3}, K_{Fe} ranges from [0.04–0.67] μmol Fe m^{-3}, R_m ranges from [2 – 3.9] d^{-1} although some values for microzooplankton in other modelling studies have suggested a lower range between [0.3–0.5] d^{-1} (see for example, Yool et al., 2013; Oliver et al., 2019), and DOM remineralisation rates range from [0.004–0.2] d^{-1} and for DOM sinking rate this range is [0.08–0.8] d^{-1}. The calibration of this model was performed through a series of experiments where parameters were varied one at a time. Each parameter was changed in this work relative to the values chosen in Bahamondes Dominguez et al. (2020) to obtain the set of parameter values that are the most representative of the wide range of processes in the CCS location. Parameter values from the control/calibrated run can be found in Table 1.

Research cruise expeditions on board the R.R.S. Discovery at the CCS location known as DY018, DY029, and DY033 were conducted during 2014 and 2015 and provide an independent dataset to validate this new model and its calibration. Model validation was done using samples collected at the CCS location during the pre-bloom, peak bloom, and post-bloom conditions of the area. The validation of this new model, updated to include a dFe pool, was done using the available data from Birchill et al. (2017). Dissolved Fe (0.2 μm filtered) was collected following GEOTRACES protocols, analysed using flow injection with chemiluminesence detection (Obata et al., 1993; Floor et al., 2015), after spiking with hydrogen peroxide (Lohan and Bruland, 2008). Full details of the methodology to obtain iron samples at the CCS location are provided in the supporting information S1 of Birchill et al. (2017).

In this model, it is assumed that during wintertime the water column is mixed and the values for dFe at the surface and in sediments are the same. Furthermore, profile data of dFe at the CCS location (Fig. 2; black-dotted line) collected during the cruises DY018 (Fig. 2a–c), DY029 (Fig. 2d–f), and DY033 (Fig. 2g–i), allow us to compare them with the daily averaged output of the model (red line). Note that the observations were collected in depth from 20 m to 140 m, therefore the first 10 m of depth are neglected in this validation. During the DY018 cruise, profiles for dFe during 11/11/2014 (Fig. 2a), 12/11/2014 (Fig. 2b), and 29/11/2014 (Fig. 2c) show relatively good agreement with the model, although dFe tends to be more repleted at the surface than in the observations. Some discrepancies are seen during the DY029 cruise where comparisons of dFe profiles (on 03/04/2015 (Fig. 2d), 16/04/2015 (Fig. 2e), and 26/04/2015 (Fig. 2f)) show the model reaching higher values over the water column in comparison to observations. This is likely due to differences in the timing of the spring bloom as shown in Fig. 4b. Yet both the data and the model show that at the onset of seasonal stratification (April), the vertical distributions of dFe are fairly uniform, with little drawdown at the surface at this stage. Finally, during the cruise DY033, profiles of dFe during 14/07/2015 (Fig. 2g), 15/07/2015 (Fig. 2h), and

Table 1
List of parameter values, including units and definitions.

Parameter	Value (Units)	References
K_{Fe}: half-saturation constant for dFe uptake	0.5 μmol Fe m^{-3}	This model
Fe_{rate}: dFe flux rate from sediments	2.5 μmol Fe m^{-2} d^{-1}	This model
Fe_{sed}: dFe at the bottom layers	1.85 μmol Fe m^{-3}	Birchill et al. (2017)
K_N: half-saturation constant for DIN uptake	0.1 mmol N m^{-3}	This model
N_{rate}: DIN flux rate from sediments	10.0 mmol N m^{-2} d^{-1}	Bahamondes Dominguez et al. (2020)
N_{sed}: DIN at the bottom layers	7.0 mmol N m^{-3}	Bahamondes Dominguez et al. (2020)
γ_1: grazing inefficiency or 'messy feeding' (0.0–1.0), returns a fraction of grazed material back into the DOM pool	0.3 (dimensionless)	Bahamondes Dominguez et al. (2020)
γ_2: fraction of dead zooplankton (0.0–1.0) that goes into the sediments	0.6 (dimensionless)	Bahamondes Dominguez et al. (2020)
λ: rate at which saturation is achieved with increasing food levels	0.007 (mmol N m^{-3})$^{-1}$	This model
R_m: maximum ingestion rate of phytoplankton	3.0 (d^{-1})	This model
m: loss rate of zooplankton due to predation and physiological death	0.01 (d^{-1})	This model
P^C_{max}: maximum value of the carbon-specific rate of photosynthesis	3.5 (d^{-1})	Moore et al. (2006) and Bahamondes Dominguez et al. (2020)
ζ: cost of biosynthesis	0.0 (mg C (mmol N)^l)	Bahamondes Dominguez et al. (2020)
α^{chl}: chlorophyll-specific initial slope of the PE curve	1.9914e−06 (mg C (mg Chl − a)$^{-1}$ (W m^{-2})$^{-1}$ s^{-1})	Moore et al. (2006) and Bahamondes Dominguez et al. (2020)
Q_m: maximum value of the cellular nutrient quota Q_{min}: minimum value of the cellular nutrient quota	0.039 (mmol N (mg C)$^{-1}$) 0.003 (mmol N (mg C)$^{-1}$)	This model This model
u_m: maximum phytoplankton carbon-specific nitrate uptake rate	0.14 (mmol N (mg C)$^{-1}$ s^{-1})	This model
θ^N_{max}: maximum value of the chlorophyll : phytoplankton nitrogen ratio	2.1 (mg Chl (mmol N)$^{-1}$)	This model
R_{ref}: respiration rate of phytoplankton	0.01 (d^{-1})	Bahamondes Dominguez et al. (2020)
rem_{DOM}: dissolved organic material or detritus-specific remineralisation rate	0.03 (d^{-1})	Edwards (2001)
w_{DOM}: sinking loss rate	0.1 (m d^{-1})	Edwards (2001)

25/07/2015 (Fig. 2i) show that during summertime there is a good agreement between the model and the observed profiles at the surface and bottom layers of the water column. Both observations and model vertical profiles show that dFe is depleted (0.1 μmol Fe m^{-3}) at the surface due to drawdown from the spring phytoplankton bloom.

Some discrepancies are shown between the modelled DIN and observed profiles of nitrate plus nitrite (Fig. 3). These differences between the model and the observations could be due to the temporal resolution of the model output as they are daily averages and the observations are samples at an instantaneous time, additionally the CTD data does not include NH_4 and the modelled DIN consider all forms of nitrogen. Fig. 3a shows a profile during the DY018 cruise (date 25/11/2014), where observations show that nitrate is still depleted at the surface by autumn, while the model shows a more mixed water column. Fig. 3b shows a profile during the DY029 cruise (date 20/04/2015), this is during the spring bloom and a depletion of nutrients at the surface is expected. Lastly, Fig. 3c shows a profile during the DY033 cruise (date 24/07/2015), showing that phytoplankton growth during summer has depleted surface DIN, however some differences can be observed between the model and the data at the bottom layers of the water column. There might be many reasons to explain the differences between observations and the model output: the NCEP reanalysis data used to force the model has a spatial resolution of 32 km, therefore some biases from the atmospheric forcing might be expected in the model; some differences in the water column temperature (not shown) during spring might account for some biases in the timing of the spring bloom and summer SST differences and for chlorophyll discrepancies during the same period (Fig. 4b). Furthermore, as shown in Fig. 6a,d,g, nutrients and chlorophyll concentrations show a large inter-annual variability during April in comparison to the months of July and August. This variability represents the inter-annual changes of the spring bloom (in terms of timing, duration, and magnitude), which makes it hard to find a parameterisation of the model that can fit all discrete and continuous observations in 2014 and 2015 not only for Chl-a but also for nutrients as they will vary depending on phytoplankton growth. Overall, we see that the tuning of our new model can capture the amplitude and timing of the nutrient and chlorophyll observations at the site of interest. We now consider the model sensitivity around this tuned state to highlight significant process features of importance at the CCS location.

Time-series of surface chlorophyll-*a* concentrations (mg Chl m^{-3}) from long-term mooring deployments including the Carbon and Nutrient Dynamics and Fluxes over Shelf Systems (CaNDyFloSS) Smartbuoy (Mills et al., 2003) were collected (Fig. 4a,b). This data was gathered during the years 2014 and 2015 as part of the research cruise expeditions DY018, DY029 and DY033.

For zooplankton comparisons, observations of zooplankton biomass were collected during four periods: 5th–12th August 2014, 10th–29th November 2014, 3rd–28th April 2015, and 13th–31st July 2015 for the cruises DY026, DY018, DY029, and DY033, respectively (Giering et al., 2018). Zooplankton were fractionated into microzooplankton, small mesozooplankton, and large mesozooplankton by using mesh sizes of 63 μm and 200 μm, hauled at 0.2 m s^{-1} and 0.5 m s^{-1}, respectively (Fig. 4c). A more detailed description of the methodology can be found in the work of Bahamondes Dominguez et al. (2020) and the complete data set can be obtained from the British Oceanographic Data Centre (BODC), (http://www.bodc.ac.uk/data) as reported in Giering et al. (2018).

Carbon-to-dry weight (C:DW; mg C (mg DW)$^{-1}$) ratios were calculated in the work of Giering et al. (2018) for different periods of the year (November 2014, April 2015, and July 2015) at the CCS location. This ratio was calculated for all size classes of zooplankton together and it allowed us to transform the modelled zooplankton biomass into mg

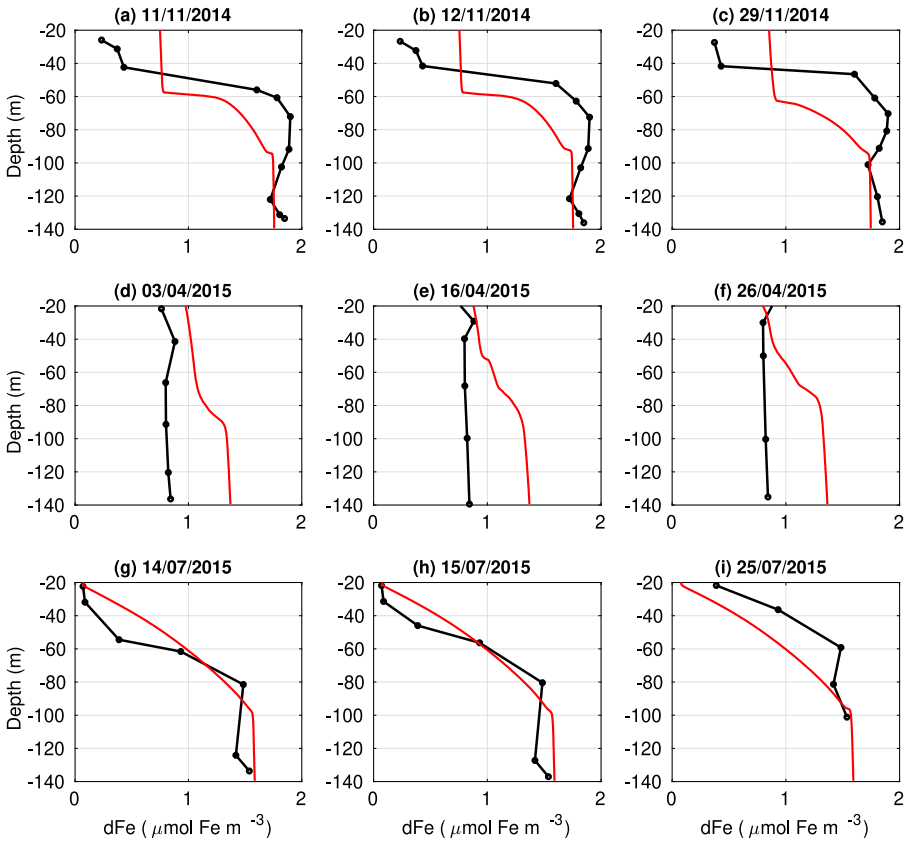

Fig. 2. Vertical profiles of dFe at the CCS location from GEOTRACES data (black-dotted line) and the model (red line) for November 2014 (a–c), April 2015 (d–f), and July 2015 (g–i). The corresponding dates for each profile are: (a) 11/11/2014, (b) 12/11/2014, (c) 29/11/2014, (d) 03/04/2015, (e) 16/04/2015, (f) 26/04/2015, (g) 14/07/2015, (h) 15/07/2015, and (i) 25/07/2015.

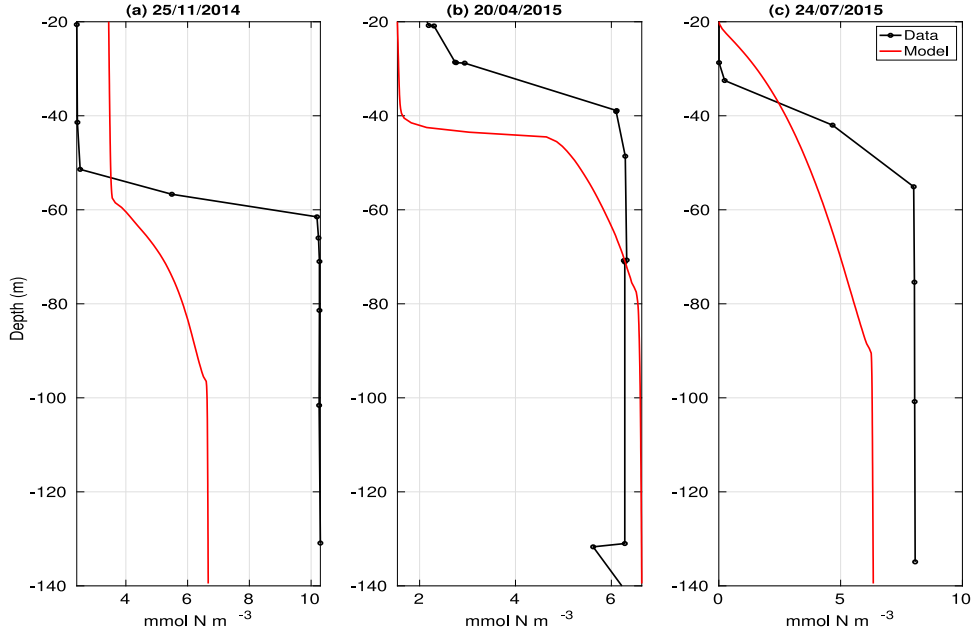

Fig. 3. Vertical profiles of the modelled DIN (red line) and CTD observations (black-dotted line) of NO_3 + NO_2 at the CCS location during (a) 25/11/2014, (b) 20/04/2015, and (c) 24/07/2015.

DW m^{-3}, so this output can be compared to the zooplankton biomass observations (Fig. 4c). This comparison shows that the spring zooplankton bloom starts approximately two months later than the spring phytoplankton bloom. Furthermore, zooplankton biomass observations show the highest values during July 2015, which matches the highest values of the modelled zooplankton biomass. However, disagreement between the calibrated model and the data exist during the sampling in 2014, a difference that could be driven by grazing dependency on temperature (Geider, 1987), a process that is not explicitly represented in the model. The lack of consecutive data over the year prevents a

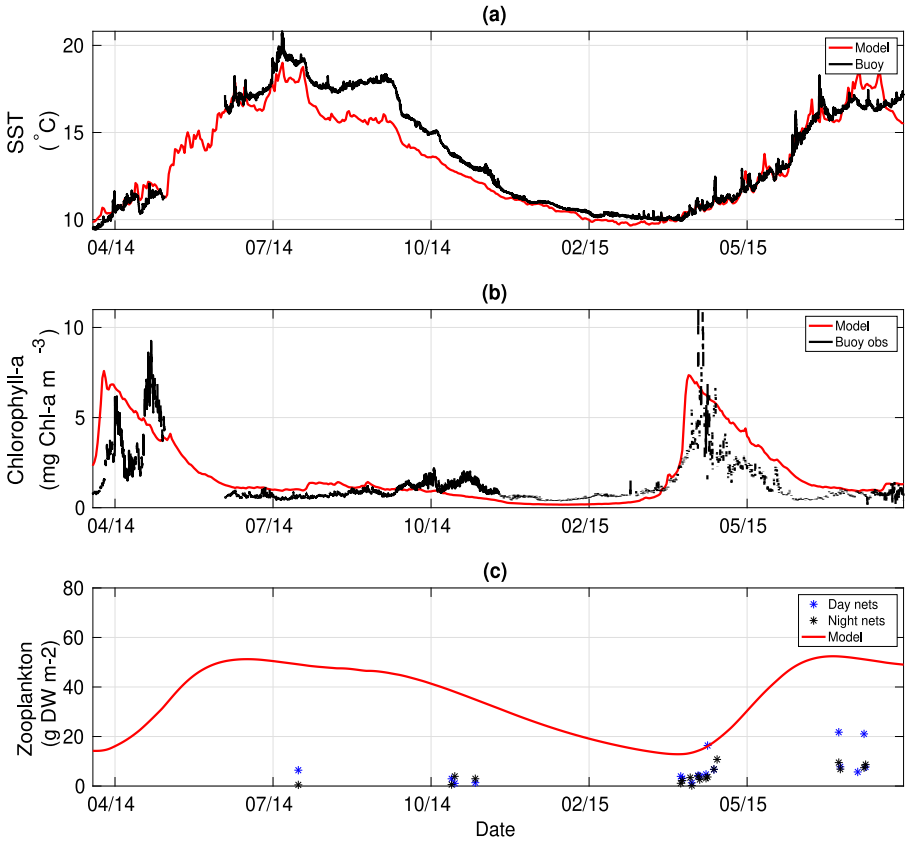

Fig. 4. SSB observations (black line) and model output (red line) for (a) sea surface temperature (SST), (b) surface chlorophyll-a, and (c) zooplankton biomass.

comparison between the model and the observations for a full seasonal cycle for zooplankton.

3. Results

3.1. Ecosystem dynamics

The modelled DIN (Fig. 5b; black line) and dFe (Fig. 5c) show that the spring bloom is mostly limited by dFe as this nutrient decreases to nearly 0 μmol Fe m^{-3} during April–May. Dissolved iron stays depleted in the surface for a short period of time until it gets remineralised at the surface and slowly starts increasing towards summertime. DIN follows a very similar seasonality to dFe, with depletion at the surface during spring and summer. However, unlike dissolved iron, DIN does not reach a total depletion during the spring bloom. During summertime and the start of the autumn period, DIN reaches a minimum at the surface (≈0.0 mmol N m^{-3}).

The modelled seasonal average depth profiles (between 1965 to 2015) of dFe, DIN, and Chl-a at the CCS location are represented in Fig. 6. These averaged vertical profiles were calculated during the months of April (green line), July (blue line), and November (red line) with their respective standard deviation (shaded area). The seasonality of dFe ranges from ≈0.2μmol Fe m^{-3} up to nearly 1.8 μmol Fe m^{-3}, showing a depletion in the surface mixed layer (SML) due to phytoplankton uptake. In the case of DIN, it shows surface depletion during spring (April) but it is during the summer month (July) that DIN reaches 0 in the first 20 m depth to almost 6.5 mmol N m^{-3} at the bottom of the water column. While chlorophyll profiles show a surface increase during April due to the spring bloom; a sub-surface chlorophyll maximum (SCM) during July, and some growth in the first 60 m depth during November, showing that during autumn there is some growth happening. It is interesting to note that the largest variability is shown during the month of April for both nutrients and chlorophyll, a pattern that makes it hard to constraint models during the spring bloom as shown in Fig. 4b. There is little variability observed for dFe and DIN during summer, however, chlorophyll shows a larger standard deviation over the whole water column, which implies that nutrients are not the only limiting factor for summer growth but in this case, it is likely due to the flexible stoichiometry of the model that allows phytoplankton to photo-acclimate to changes in light.

Estimations of daily rates of PP in the Celtic Sea have been reported in the range of 100 to 600 mg C m^{-2} d^{-1} in the summer months (Joint and Pomroy, 1983; Holligan et al., 1984; Joint et al., 1986; Maranon et al., 2005; Hickman et al., 2012). Curran et al. (2018) used satellite ocean-colour based models to estimate the total daily integrated PP in the Celtic Sea in April to range between 600–1700 mg C m^{-2} d^{-1}. These observed PP estimates are higher than the modelled values (Fig. 7a,b) during the spring bloom, however, this could be due to sub-optimal parameterisation in the satellite PP estimation process (Brewin et al., 2017).

3.2. Co-limitation of nutrients for phytoplankton growth

This paper focuses on investigating the nutrient co-limitation of phytoplankton growth at the CCS location. This is analysed in Fig. 8 by comparing N_{lim} (red line), Fe_{lim} (black line), and normalised chlorophyll-a (blue line) at the surface (0–1 m depth) and sub-surface (20 m depth). The normalised chlorophyll-a (normChl) was calculated as:

$$normChl = \frac{Chl - min(Chl)}{max(Chl) - min(Chl)}.$$

Fig. 8a shows that the seasonal range of N_{lim} goes from ≈0.0 to ≈0.98. In the case of Fe_{lim}, the range of values is smaller than for N_{lim}, ranging from ≈0.05 to ≈0.7. As shown in Fig. 5, dFe only gets depleted during springtime (April, May), while the rest of the year the

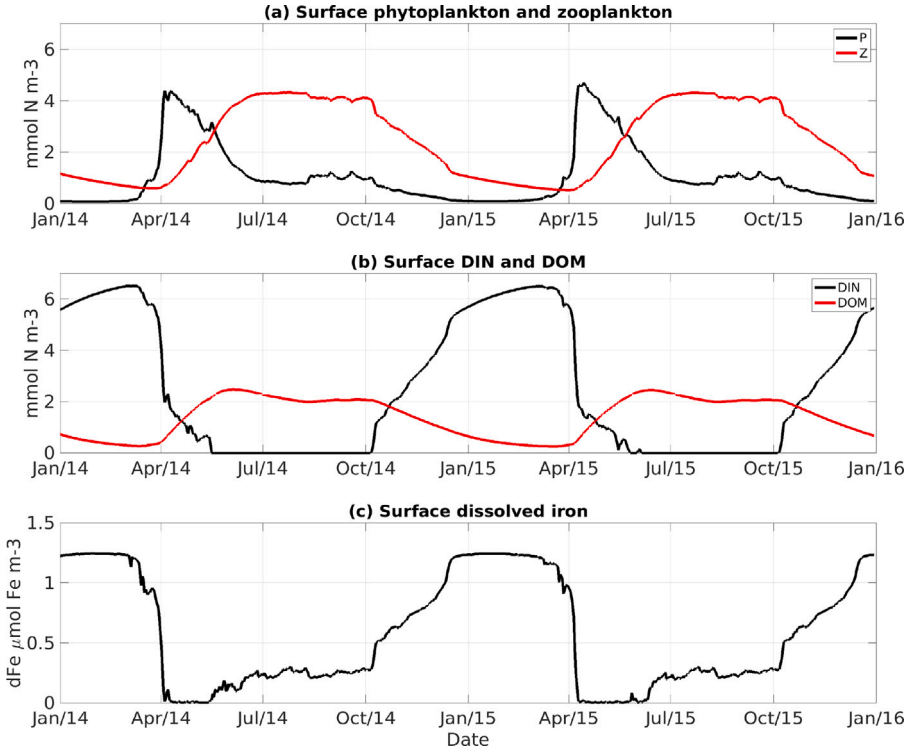

Fig. 5. Control model representation of the surface seasonal cycle at the CCS location during 2014 and 2015 for (a) phytoplankton biomass (P; black line) and zooplankton biomass (Z; red line); (b) DIN (black line) and DOM (red line); and (c) dFe.

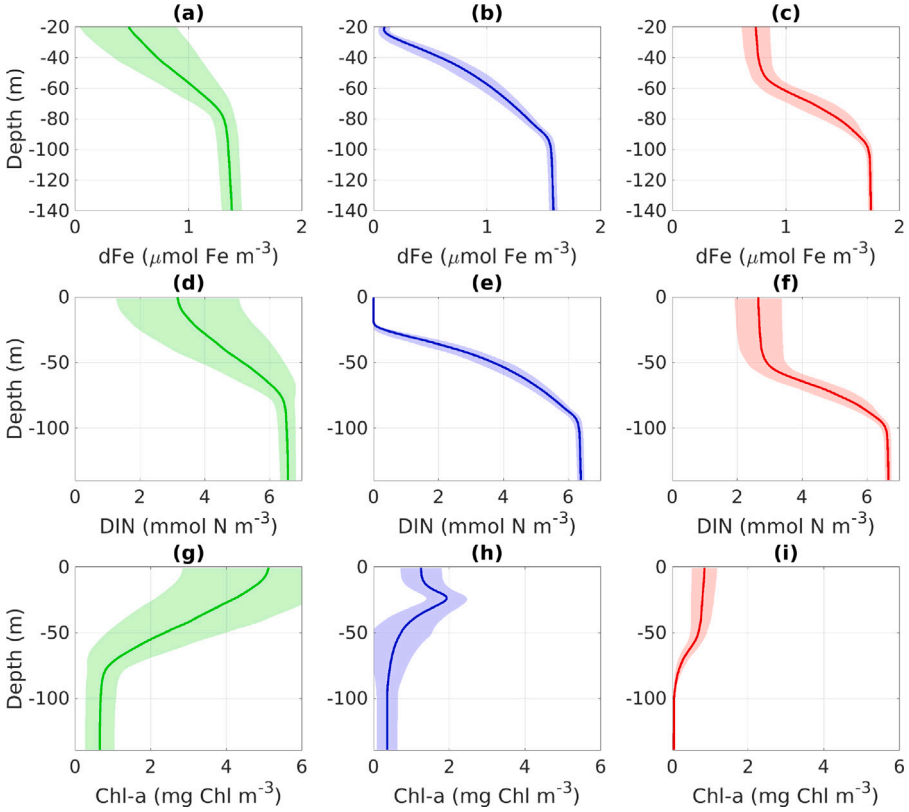

Fig. 6. Monthly average profiles from 1965–2015 for April (green line), July (blue line), and November (red line) for dFe (a, b, c), DIN (d, e, f), and Chl-a (g, h, i). Shaded colours represent the standard deviation over the simulated period of the model for April (green), July (blue), and November (red).

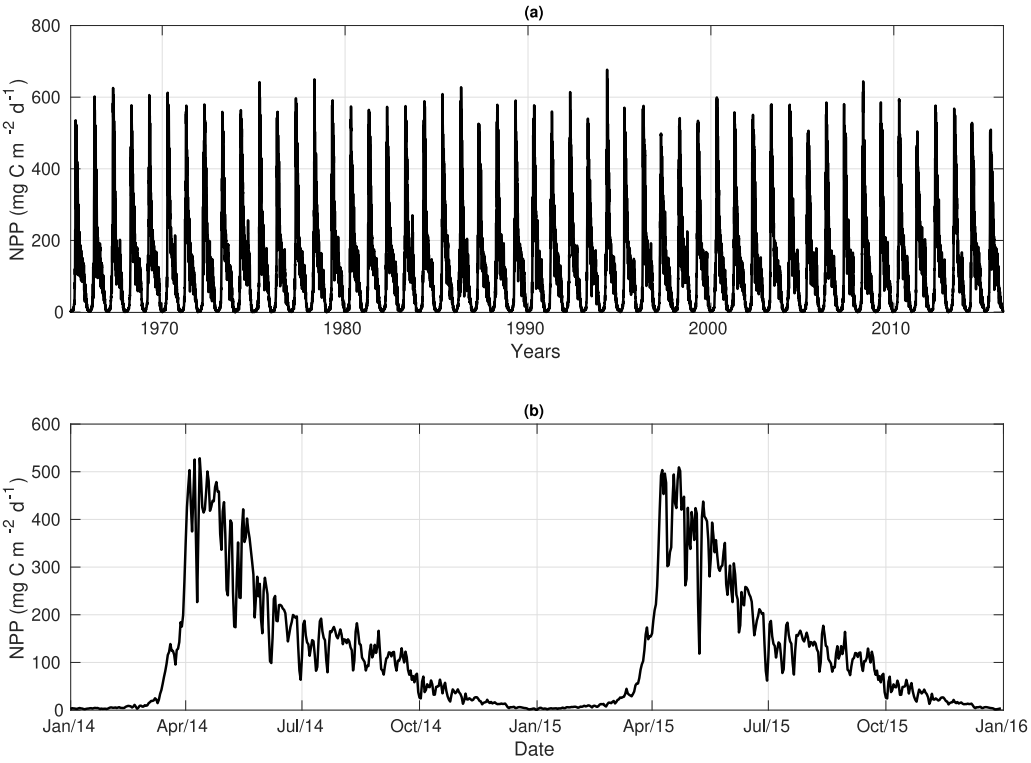

Fig. 7. Net primary production (NPP) output from the control model at the CCS locations during the years (a) 1965–2015, and (b) 2014–2015.

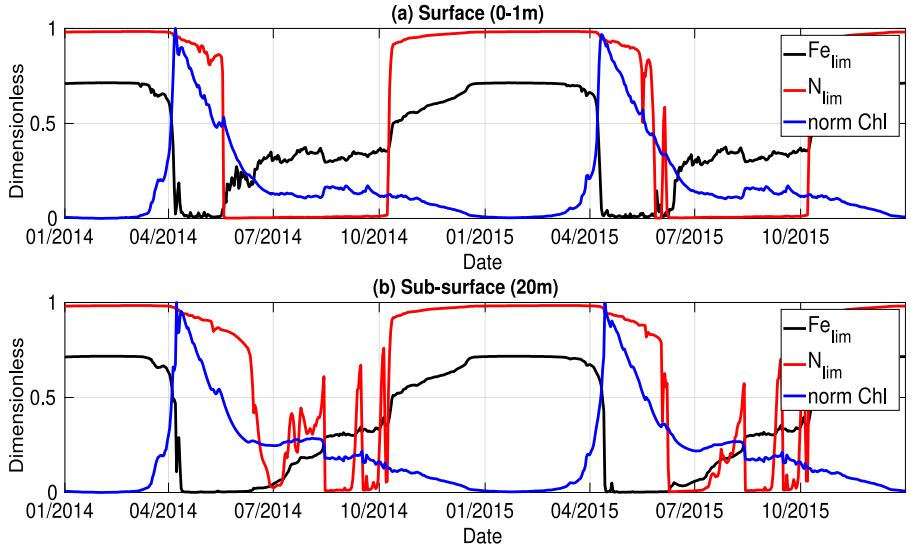

Fig. 8. Daily time-series from the control run for years 2014 and 2015 for N_{lim} (red line), Fe_{lim} (black line), and normalised chlorophyll-a (blue line) at (a) surface (0–1 m depth), and (b) sub-surface (at 20 m depth).

model shows that phytoplankton growth is primarily limited by DIN. Furthermore, Fig. 8b shows that in the sub-surface during summertime N_{lim} varies more than in comparison to the surface, providing short periods of time between July–September where dFe is a more limiting nutrient than DIN. During this time, phytoplankton biomass increases, showing that the 1-D model can reproduce a SCM, which is likely supported by nutrient entrainment through the thermocline.

Fig. 9a and b show that the nutrient limitation for phytoplankton growth changes over time but also through depth. However, the major changes occur at the top 60 m depth, where phytoplankton is able to grow. The difference between Fe_{lim} and N_{lim} (Fig. 9c) explicitly represents which nutrient is limiting at a certain time and depth. During the months of April–July, phytoplankton growth (Fig. 9d) shows to be primarily limited by dFe at all depths. However, it is clear that DIN becomes more limiting during the summer period at the surface (0–30 m depth). This seasonal nutrient co-limitation pattern is observed during the 50-year model simulation (see Fig. A.1), with the standard deviation of (Fe_{lim} - N_{lim}) difference (grey-shaded area) showing that the largest inter-annual variability of nutrient co-limitation occurs during the start and end of the spring bloom, possibly driven by inter-annual variability in the timing of the bloom.

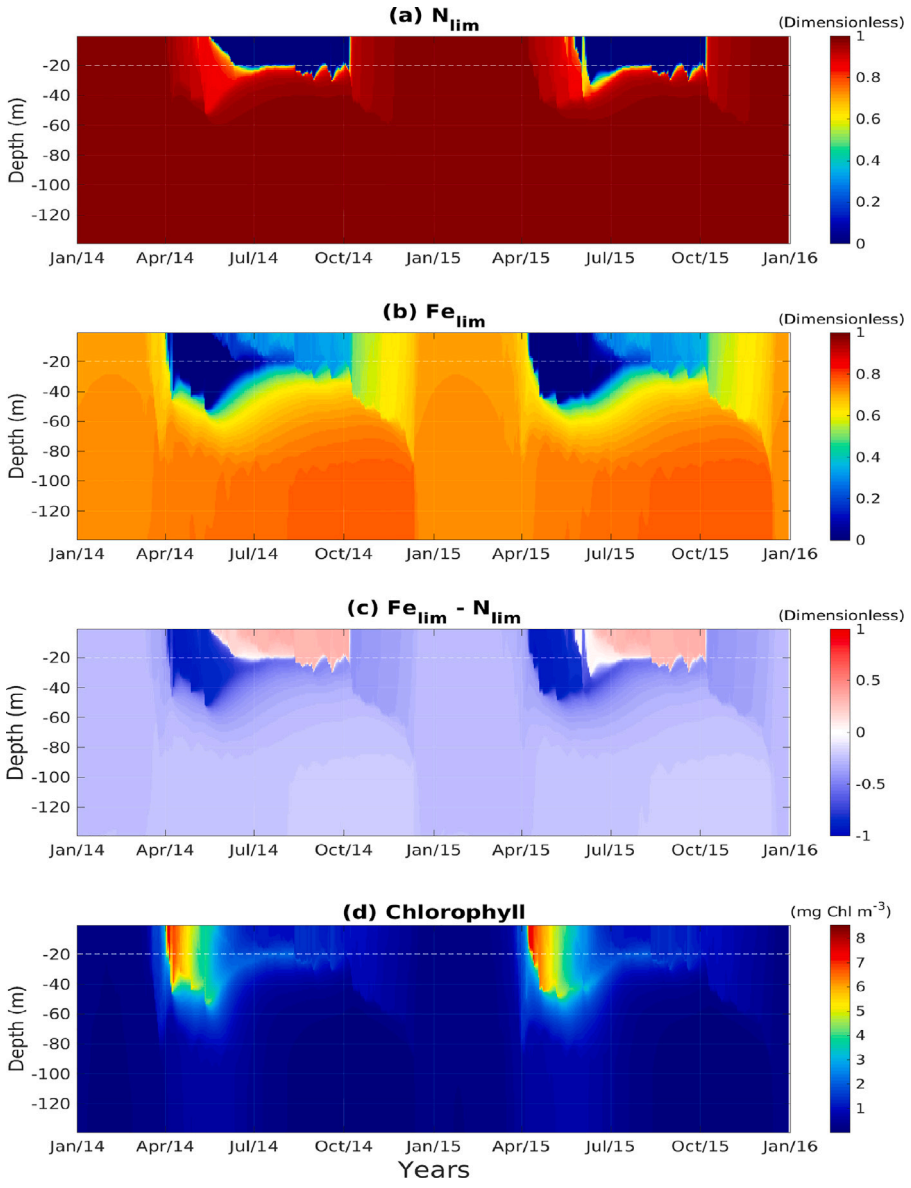

Fig. 9. Daily time-series through depth during the years 2014 and 2015 for (a) N_{lim}, (b) Fe_{lim}, (c) the difference of Fe_{lim} and N_{lim}, and (d) chlorophyll.

3.3. Sensitivity studies

A sensitivity analysis was performed to assess the importance of nutrient-associated parameters, including the remineralisation rates of dFe (Fe_{rate}) and DIN (N_{rate}) as well as the two parameters that modify nutrient assimilation: the half-saturation constants of dissolved iron and DIN (K_{Fe} and K_N, respectively). Two sets of experiments were created: an ensemble of values for K_N and K_{Fe} have been chosen for the known range from the literature, taking into account the minimum and maximum values of these ranges as suggested in Section 2.2; the second set of sensitivity experiments varied the nutrient benthic rate parameters from their calibrated value (see Table 1) by ±50%. The design of this sensitivity experiment ensemble for the four different parameters was dependent on the known values and ranges from the literature, including models and observations, however, there were insufficient observations for N_{rate} and Fe_{rate} to provide a reliable range of values. Each experiment is listed in Table 2, where each parameter was varied individually to understand how sensitive NPP is to those changes and the effect that they have on the nutrient co-limitation of the CCS location. The control experiment in this section corresponds to the calibrated model shown in the methodology.

Table 2
Sensitivity experiments to nutrient related parameters for dFe and DIN. Control value corresponds to the calibrated value found for each parameter as seen in Table 1.

K_N	Value	K_{Fe}	Value	N_{rate}	Value	Fe_{rate}	Value
Exp1	0.5	Exp7	0.04	Exp13	5.0	Exp15	1.25
Exp2	0.9	Exp8	0.15	Exp14	15.0	Exp16	3.75
Exp3	1.3	Exp9	0.25				
Exp4	1.7	Exp10	0.35				
Exp5	2.1	Exp11	0.45				
Exp6	2.5	Exp12	0.67				
Control	**0.1**	**Control**	**0.5**	**Control**	**10.0**	**Control**	**2.5**

These results show that the ensemble of sensitivity experiments for K_N (Exps 1–6) produce the largest variability in N_{lim}^{perc} reflected at different depths (Fig. 10), suggesting a linear increase on the number of points (depths/days) that are N-limited instead of Fe-limited when the half-saturation of DIN is higher, an expected behaviour according to the definition of nutrient co-limitation (see Eqs. (5),(6)). On the other hand, the range of values tested for K_{Fe} (Exps 7–12) shows less variability for N_{lim}^{perc} (Fig. 10), suggesting that in the lower range

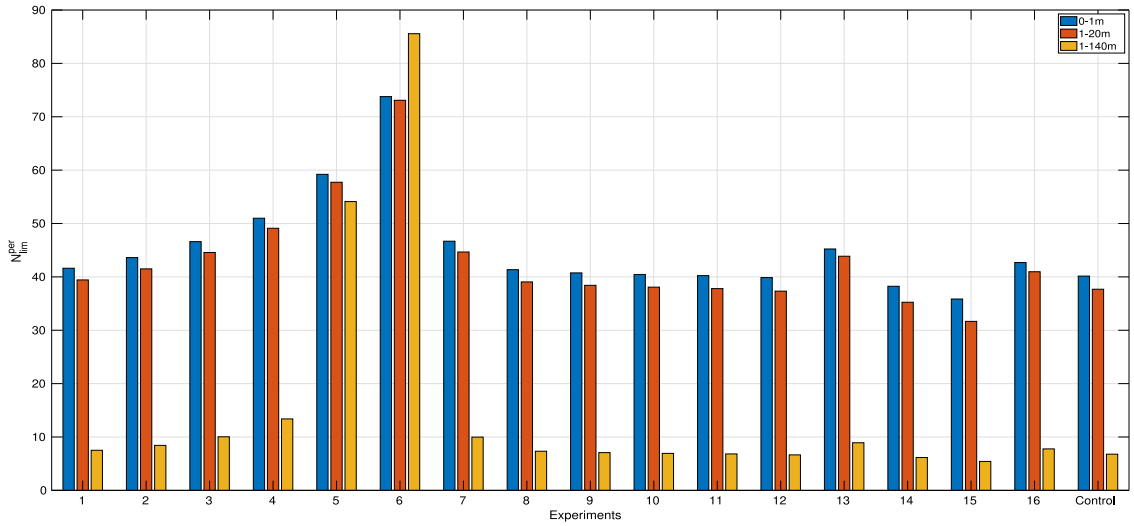

Fig. 10. Control run and sensitive experiments for N_{lim}^{perc} in different depths: surface (0–1 m), subsurface (1–20 m), and full depth (1–140 m).

of values (e.g., K_{Fe} = 0.04 μmol Fe m^{-3}), shows a slight increase in N_{lim}^{perc}. For the benthic nutrient parameters (Exps 13–16), decreasing or increasing N_{rate} and Fe_{rate} will lead to lower and higher DIN and Fe availability for phytoplankton growth, respectively. The result is that a decrease in N_{rate} leads to more points in depth and days being N-limited than Fe-limited (i.e. higher N_{lim}^{perc}). A similar response is shown for a decrease in Fe_{rate}, which decreases N_{lim}^{perc} as less dFe available at the surface will imply more Fe-limiting points at depth/days.

Changes for N_{lim} and Fe_{lim} for each sensitivity experiment are shown in Figs. 11–12. Exps1-6 show that changes in the K_N parameter produces variability in N_{lim} (Fig. 11a), where an increase in the half-saturation constant of DIN will decrease N_{lim} between the months of October to approximately June of the following year. No changes are observed when the system is N-limited (June–October). On the other hand, negligible differences for N_{lim} occur when changing the values of K_{Fe} (Fig. 11b). Changes in the nutrients benthic rates (Fig. 11c,d) can impact the co-limitation timing (varying from an ecosystem being Fe-limited into N-limited as shown in Fig. 8). These experiments can also change nutrient availability which alters the uptake of nutrients for phytoplankton growth. Increasing Fe_{rate} replenishes dFe at the sub-surface, making DIN more limiting at an earlier stage (Fig. A.2d). The opposite behaviour is observed when decreasing Fe_{rate} by 50%. Similar changes for N_{lim} occur when changing N_{rate} (Fig. A.2c) but the impact of Exps 13–16 is greater at the sub-surface (Fig. A.2c,d).

Variations of the K_N parameter have little effect on Fe_{lim} (Fig. 12a), while Exps7-12 show great sensitivity to changes in K_{Fe} (Fig. 12b): when K_{Fe} is increased, then Fe_{lim} decreases and dFe becomes more limiting for phytoplankton growth. Changes in iron limitation, when changing the magnitude of Fe_{lim}, largely occur over the year except during the spring bloom but the timing for when the system becomes more Fe-limited shows little variability in the sensitivity experiments. This suggests that the results showing that the spring bloom is mainly Fe-limited are robust. On the other hand, similar to the behaviour observed for Exps13-16 (varying N_{lim}) (Fig. 11), variations in N_{rate} and Fe_{rate} can produce small differences in the magnitude of Fe_{lim} however the timing of Fe-limitation will depend on these parameters, with their impact being stronger in the sub-surface (Fig. A.3c,d).

To further investigate the effects of the sensitivity experiments on nutrient co-limitation and the whole system, Fig. 13 shows the difference in depth integrated NPP between each sensitivity experiment and the control run. Despite the direct impact that changes in the parameters K_N and K_{Fe} have on N_{lim} and Fe_{lim} (Figs. 11a,b, 12a,b), respectively, NPP is not as sensitive to those parameters (Fig. 13a,b) as it is to varying the nutrient benthic parameters (Fig. 13c,d). This response of NPP to the sensitivity studies can also be reflected in the total annual NPP (Fig. A.4), with little changes for the Exps 1–12. Changes in N_{rate} and Fe_{rate} will directly affect the nutrient availability in the water column, impacting phytoplankton productivity through changes in the timing of the spring bloom and the magnitude of summer growth. This variability in NPP can potentially explain the changes in the timing of the system being more Fe-limited or N-limited (Figs. 11c,d, 12c,d).

4. Discussion

4.1. Ecosystem dynamics and nutrient co-limitation

In temperate shelf seas such as the Celtic Sea, the seasonal cycle starts with a mixed and homogeneous water column in winter but towards spring the increase of solar radiation heats the surface waters, making them more stable by lowering the density of the water at the surface and reducing convective mixing (Taylor and Stephens, 1993; Ruiz-Castillo et al., 2019). The vertical net heat flux becomes positive in early spring, producing a state of net heating in the surface waters. This stabilises the water column and allows the start of thermal stratification, which intensifies the net growth rate of phytoplankton due to increased irradiance, initiating the spring phytoplankton bloom (Kanda et al., 1989; Fig. 5a). This spring phytoplankton bloom terminates due to the grazing pressure exerted by zooplankton (Fig. 5a) and the depletion of nutrients (Fig. 5b,c). This dynamical feedback between growth, death, and grazing between phytoplankton and zooplankton is represented by the seasonality of DOM (Fig. 5b), which increases due to respiration losses of phytoplankton, zooplankton mortality, and sloppy feeding.

Zooplankton is represented in this model using one functional group that represents the whole community of zooplankton in the CCS location. Zooplankton is an important energy pathway between the base of the food chain and higher trophic levels such as fish, birds and mammals, but the impact they have on chemical cycling in the ocean is also well-documented (Buitenhuis et al., 2006; Turner, 2015; Steinberg and Landry, 2017). In Fig. 4c, a comparison of zooplankton biomass between observations and the model show differences. And while we acknowledge that evaluating the accuracy of zooplankton abundance or biomass in numerical experiments is a major challenge due to the sparse ship-based observations in most regions (Everett et al., 2017; Shropshire et al., 2020), the ecological role of zooplankton should not be underestimated. However, the differences in simulated zooplankton could be due to many reasons, influenced by the number of functional

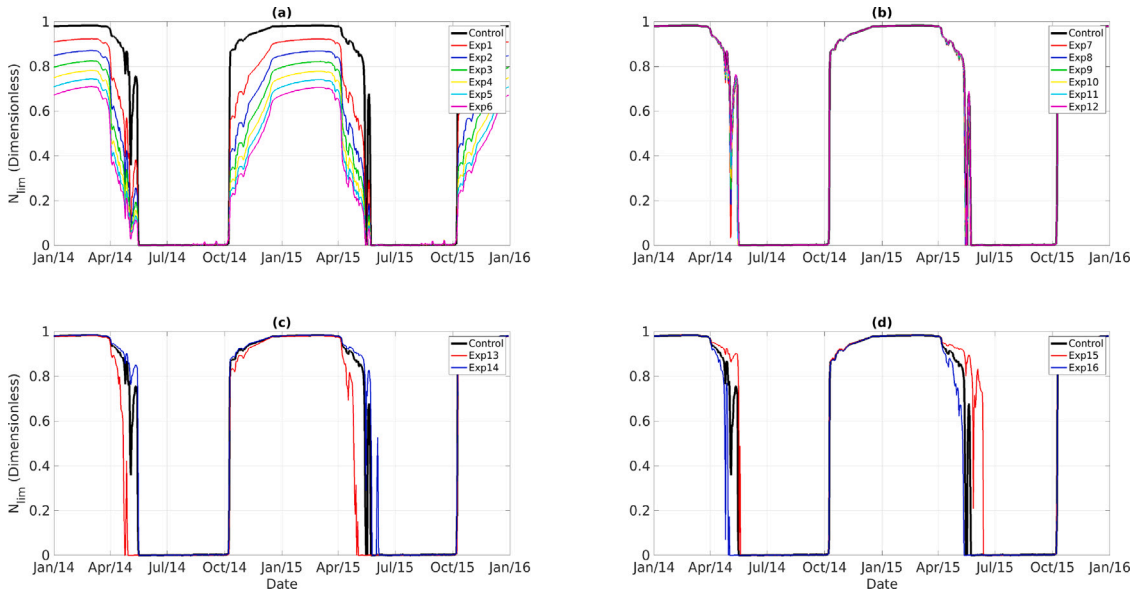

Fig. 11. Surface N_{lim} for 2014 and 2015 for (a) K_N experiments (Exps 1–6), (b) K_{Fe} experiments (Exps 7–12), (c) N_{rate} experiments (Exps 13–14), and (d) Fe_{rate} experiments (Exps 15–16). The control run is represented in a black line in every subplot.

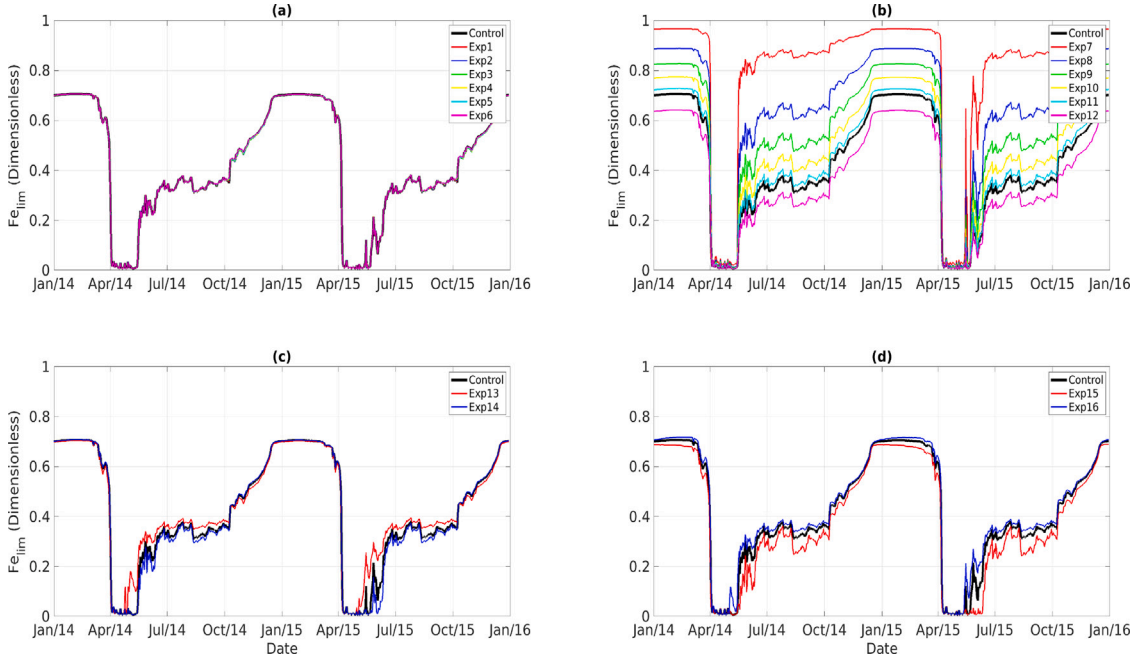

Fig. 12. Surface Fe_{lim} for 2014 and 2015 for (a) K_N experiments (Exps 1–6), (b) K_{Fe} experiments (Exps 7–12), (c) N_{rate} experiments (Exps 13–14), and (d) Fe_{rate} experiments (Exps 15–16). The control run is represented in a black line in every subplot.

types (only one in this work) or the chosen mathematical grazing function. Based on 153 published biogeochemical models, Arhonditsis and Brett (2004) found that 95% of them compared output with phytoplankton data, but <20% compared model output with zooplankton data. Validating zooplankton dynamics in physical–biological coupled models such as the one in this study is key to increasing confidence in model solutions, but there needs to be greater discussion and collaboration between modellers and observationalists for this comparison to improve (Flynn, 2005).

On the other hand, the model shows that once the spring bloom starts, a depletion of nutrients at the surface occurs due to phytoplankton uptake (Fig. 5) but a sustained growth of phytoplankton during summer is also observed. This summer growth could likely be a consequence of an entrainment of nutrients to the surface layers through the thermocline as shown by previous studies (Dugdale and Goering, 1967; Holligan et al., 1984; Hickman et al., 2012). This nutrient-fuelled production during summer is likely driven by the tidal regime at the CCS location, such as a spring–neap tidal cycle (Sharples, 2008), and a variability in winds (Eslinger and Iverson, 2001). Additionally, tidal turbulence increases during spring tides in comparison to neap tides, modifying the base of the thermocline (Sharples, 2008). On the other hand, during the spring bloom the nutrient co-limitation observed in this work (Figs. 8, 9) shows that phytoplankton is mainly limited by dFe. Dissolved iron reaches a minimum value at the surface but

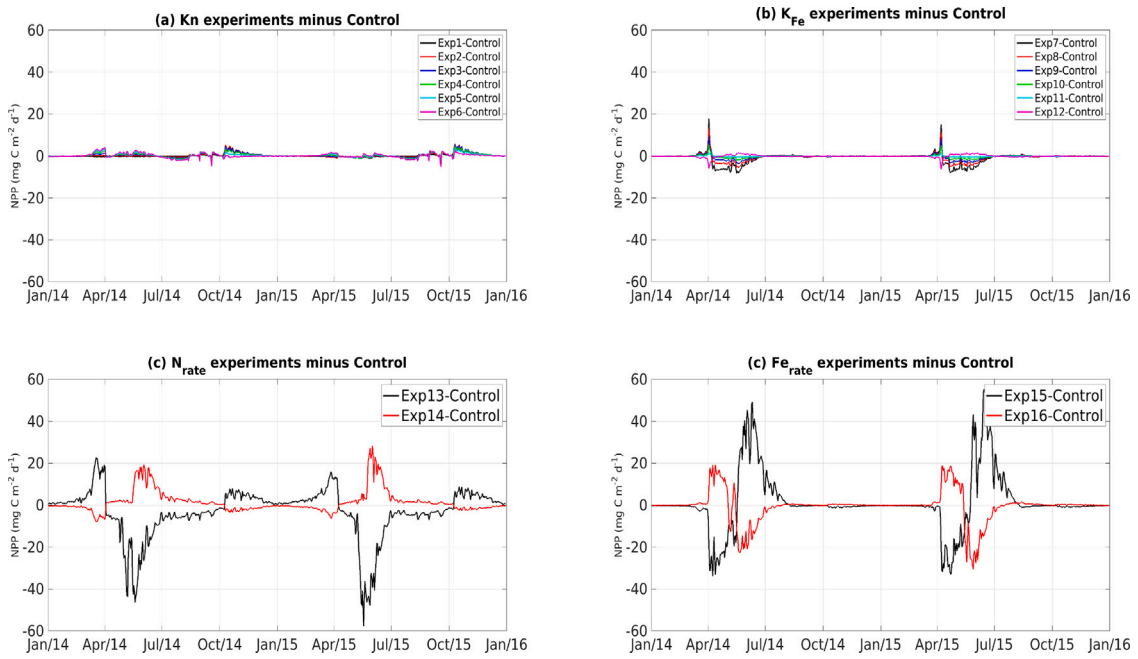

Fig. 13. Difference of depth-integrated NPP for 2014 and 2015 between each sensitivity experiment and the control run, considering (a) K_N experiments (Exps 1–6), (b) K_{Fe} experiments (Exps 7–12), (c) N_{rate} experiments (Exps 13–14), and (d) Fe_{rate} experiments (Exps 15–16).

increases in summer and during autumn (Fig. 5c), likely due to longer and more frequent wind events increasing surface mixing (Williams et al., 2013b; Fig. 6c,f,i). Episodic pulses of wind can deepen the thermocline, entraining nutrients from the bottom mixed layer into the surface mixed layer (Yin et al., 1995). During winter, nutrient limitation for phytoplankton growth becomes secondary to light limitation as the mixed layer is relatively deep and phytoplankton spend a large proportion of their time in waters with insufficient light to support photosynthesis (Smith et al., 2015).

This work shows that dissolved iron is an essential nutrient at the CCS location for the initiation of the spring bloom, but summer growth is mainly sustained by DIN (Fig. 9). Similar results as the ones from this work have been found for certain regions such as the Arctic, where phytoplankton productivity is limited by nitrogen once the spring bloom is complete (Mills et al., 2018). While other studies have found that N and Fe are co-limiting nutrients in many regions, such as the California Current System, which for several decades was generally described as being nitrogen limited. However, observations in this region (Johnson et al., 1997; Hutchins and Bruland, 1998) suggest that dissolved iron also plays a key role for phytoplankton growth (King and Barbeau, 2007). In the CCS location, previous studies confirm that the summer N-limitation for phytoplankton growth will depend on the vertical distribution of DIN and light availability, and the subsequent ability of phytoplankton to photo-acclimate to these changes (Hickman et al., 2009; Birchill et al., 2017). Because the S2P3 v8.0 considers a flexible stoichiometry (Bahamondes Dominguez et al., 2020), it allows phytoplankton to acclimate to environmental changes, a process that could explain a larger variance observed in summer for chlorophyll in comparison to DIN and dFe (Fig. 6b,e,h). This suggests that during the summer months, besides nutrient availability, light variability could also have an impact on phytoplankton growth. The results shown in this work are similar to those in Birchill et al. (2017) in terms of nutrient co-limitation, but S2P3 v8.0 allows us to have a deeper look into the ecosystem dynamics of the CCS location and to understand the underlying processes that allow DIN and dFe to co-limit phytoplankton growth.

4.2. Sensitivity studies

The Celtic Sea has been the focus of many studies regarding nutrient cycling and the availability of DIN to phytoplankton (Pingree et al., 1976; Sharples et al., 2001; Hickman et al., 2012; Williams et al., 2013a) but Birchill et al. (2017)'s work demonstrated the importance of iron at the CCS location, showing that phytoplankton growth is co-limited by DIN and dFe. This shelf sea is a physically dynamic environment with high values of PP, where the combination of sediment resuspension (Nédélec et al., 2007; Elrod et al., 2008) and a diffusive flux of Fe (Dehairs et al., 1989; Santschi et al., 1990; Elrod et al., 2004; Ussher et al., 2007; Lohan and Bruland, 2008) can lead to shelf sediments being a significant source of Fe to the surface waters. During winter, in temperate shelf seas such as the Celtic Sea, the water column is kept vertically homogeneous by convective overturning, allowing a whole-depth mixing of water constituents such as phytoplankton cells and inorganic nutrients (Simpson and Sharples, 2012). Therefore, vertical mixing during winter can supply DIN and dFe to the photic zone, whilst vertical diffusion across the seasonal thermocline supplies nitrate to the photic zone during the summer (Rippeth et al., 2005). Deep convective mixing has been shown to be the dominant mechanism for nutrient supply to surface waters; remineralisation of dFe from the sediments can supply at least 4–10 times more dFe to surface waters than other Fe sources (aeolian deposition, vertical diffusive fluxes, and horizontal surface fluxes) (Birchill et al., 2019). This is what the sensitivity experiments show in this work: the benthic fluxes for DIN and dFe have a great impact on phytoplankton productivity. It is also important to not neglect the impact that the half-saturation constants have on the system being more Fe-limited or more N-limited during the season for phytoplankton growth.

Phytoplankton carbon fixation can be influenced by the concentration of other inorganic nutrients in the photic zone (nitrogen, phosphorus, silicon, etc.) as phytoplankton growth tends to uptake nutrients in stoichiometric proportions (Redfield et al., 1963; Heath and Beare, 2008). Therefore, phytoplankton production will depend on the rate of supply of all nutrients to the photic zone through advection, convection, mixing, diffusion, atmospheric input, or organic material recycled

from excretion and microbial activity. One rate of supply to the DIN and dFe pools comes from DOM decay or remineralisation (rem_{DOM}, see Table 1). It is important to note that the detrital decay rate will depend on the type of detritus being simulated, while some intermediate complex models consider the flow of organic material to detrital pools, both a slow- and a fast-sinking pool, the inclusion of detritus in this model represents all types of detritus in one pool. As some other studies have shown before, changes in the detrital decay parameter will produce a linear response from the system, producing variations in the concentration of detritus in the water column (Macdonald et al., 2009). A sensitivity experiment of the parameter rem_{DOM} would affect the nutrient concentrations (Kriest et al., 2010). For example, reducing rem_{DOM} should also decrease the concentrations of DIN and dFe in the water column. Therefore, changes in the nutrient concentrations are not only due to PP, zooplankton excretion, or the benthic supply of DIN and dFe, but also due to decay of detritus. Many studies have shown the sensitivity of different regions of the ocean to changes in rem_{DOM} (Powell et al., 2006; Macdonald et al., 2009; Kriest et al., 2010; Hasumi and Nagata, 2014), and we would expect to see the same behaviour in this work, so this is not replicated in this study.

Appropriate parameterisations to represent shelf seas are connected to the available observations. Shelf seas are both physically dynamic and highly productive regions (Simpson and Sharples, 2012) and many parameters are poorly constrained due to the lack of available reference datasets. Shelf sediments are one of the major sources of nutrients to the overlying water column (Nédélec et al., 2007; Elrod et al., 2008), but little is known about the atmospheric or aeolian input for dFe at the CCS. Future work could add this input to the model using available reference data for calibration.

4.3. Future model development

Considering multiple species of phytoplankton in biogeochemical modelling has become more relevant due to the impact increasing complexity has on projections. dFe does not only influence phytoplankton growth, but the ecosystem structure (Landry et al., 2000; Tsuda et al., 2003), as each phytoplankton species has differing Fe requirements which can alter uptake efficiencies (Öztürk et al., 2004; Lis et al., 2015). It is acknowledged in this work that further sophistication of the model can lead to poorly constrained scenarios due to the larger amount of parameters that need to be validated. However, the collection of more observations that tackle the nutrient requirements for different phytoplankton in temperate shelf seas can aid to better understand and model the response of the ecosystem to nutrient co-limitations.

5. Conclusions

The supply of macronutrients (that contain bioavailable N, P or Si) and several micronutrients (trace metals, vitamins) largely determines phytoplankton production in the ocean (Li et al., 2015). Amongst these limiting elements, N and Fe have been identified for having key roles in limiting PP (Martin et al., 1991; Falkowski, 1997). This study investigates a recently discovered co-limitation of nutrients (DIN and dFe) for phytoplankton growth in the Central Celtic Sea location. Birchill et al. (2017) first suggested this co-limitation between DIN and dFe and here we extend on this work through a modelling approach. The model is able to reproduce the whole seasonal cycle over 51 years with daily resolution, allowing us to understand the nutrient co-limitation of phytoplankton growth in more detail. These results are robust and allow us to show when the region is Fe-limited (spring) or N-limited (summer).

This work shows that a seasonal cycle for dFe and DIN is evident for the CCS location. The nutrient distribution in shelf seas is controlled by the seasonal dynamics of the region (Liu et al., 2000; Roughan and Middleton, 2002; Ruiz-Castillo et al., 2019) and, with changes in the seasonal stratification for the North West European shelf sea projected to increase by 20% (Holt et al., 2010), understanding the dynamical feedbacks between two limiting nutrients for phytoplankton growth in the Celtic Sea becomes important.

Changes in the patterns of upper-ocean nutrient limitation could be influenced by a range of processes in the future. An increase of anthropogenic carbon dioxide can alter the surface ocean chemistry but, at the same time, climate–ocean feedbacks can potentially change atmospheric carbon dioxide concentrations via oceanic nutrient cycles and the biological carbon pump (Moore et al., 2013). This model and the technique used to understand nutrient co-limitation has been demonstrated to be a useful tool that could be applied in other regions where there is iron limitation, such as high latitude regions. Alternatively the model could be used in oceanic regions where it has been previously thought that iron is not a limiting nutrient for PP in order to test this assumption. Understanding of existing patterns of nutrient limitation and co-limitation could be used to provide answers for possible future changes and projections of how biological communities will respond or influence nutrient availability.

CRediT authorship contribution statement

Angela A. Bahamondes Dominguez: Writing – original draft, Investigation, Conceptualization, Visualization, Model development, Validation, Calibration. **Helen S. Macdonald:** Model development, Supervision, Writing – review & editing. **Graham Rickard:** Model development, Supervision, Investigation, Writing – review & editing. **Matthew L. Hammond:** Visualization, Statistical analysis, Writing – review & editing.

Declaration of competing interest

The authors declare that they have no known competing financial interests or personal relationships that could have appeared to influence the work reported in this paper.

Data availability

Data will be made available on request.

Acknowledgements

Antony Birchill is thanked for the original collection, generation, discussion, and interpretation of the dissolved iron data. Biological observations used for the model validation were acquired through the Natural Environment Research Council (NERC) funded UK Shelf Sea Biogeochemistry (SSB) research programme.

Funding

This work was funded by the MBIE NZ project code ANTA1801 aligned by the Antarctic Science Platform (ASP), New Zealand.

Appendix

See Figs. A.1, A.2, A.3 and A.4.

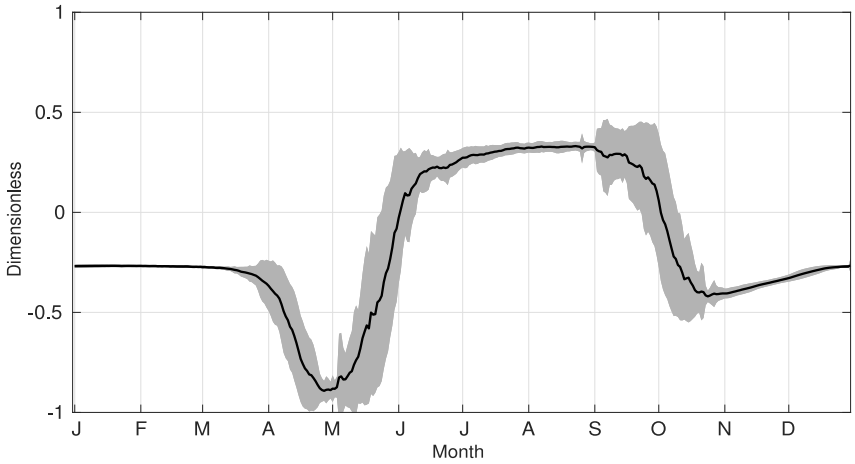

Fig. A.1. Difference between daily surface values of Fe_{lim} and N_{lim} averaged for 1965–2015 (black line) and standard deviation over the same period (grey shaded area).

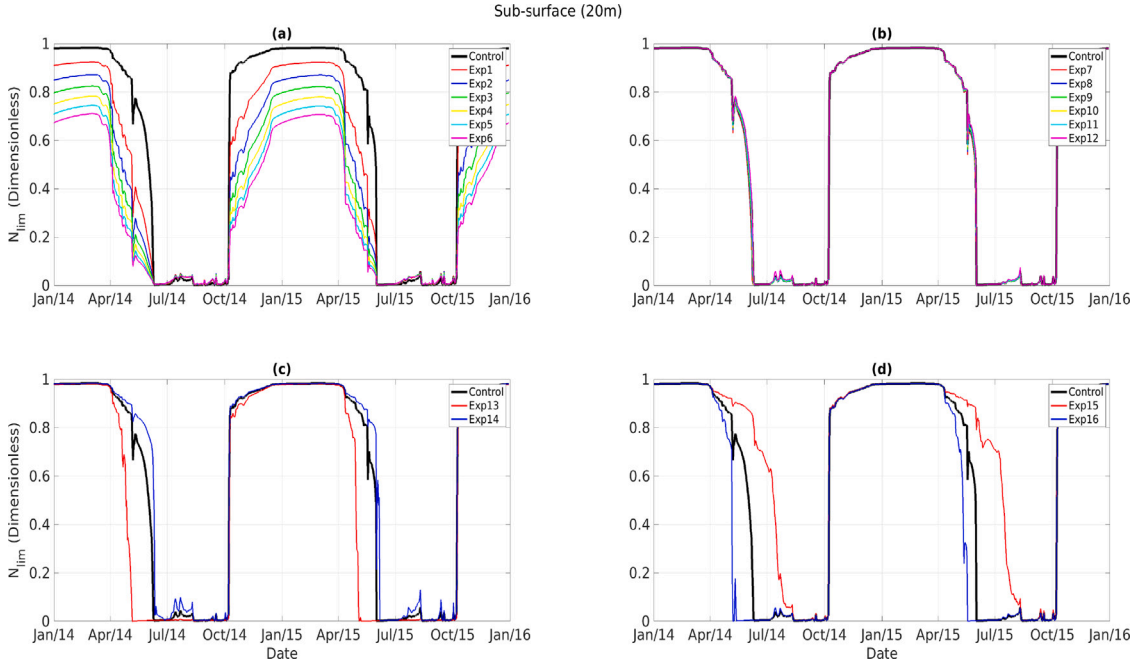

Fig. A.2. Sub-surface (20 m depth) N_{lim} for 2014 and 2015 for (a) K_N experiments (Exps 1–6), (b) K_{Fe} experiments (Exps 7–12), (c) N_{rate} experiments (Exps 13–14), and (d) Fe_{rate} experiments (Exps 15–16). The control run is represented in a black line in every subplot.

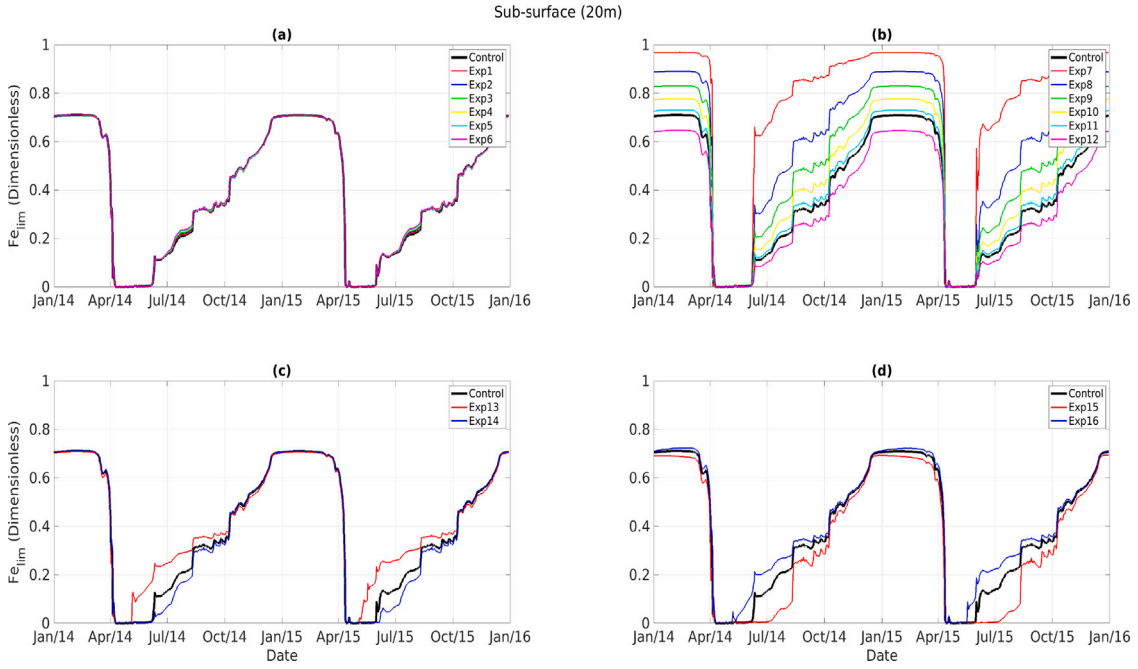

Fig. A.3. Sub-surface (20 m depth) Fe_{lim} for 2014 and 2015 for (a) K_N experiments (Exps 1–6), (b) K_{Fe} experiments (Exps 7–12), (c) N_{rate} experiments (Exps 13–14), and (d) Fe_{rate} experiments (Exps 15–16). The control run is represented in a black line in every subplot.

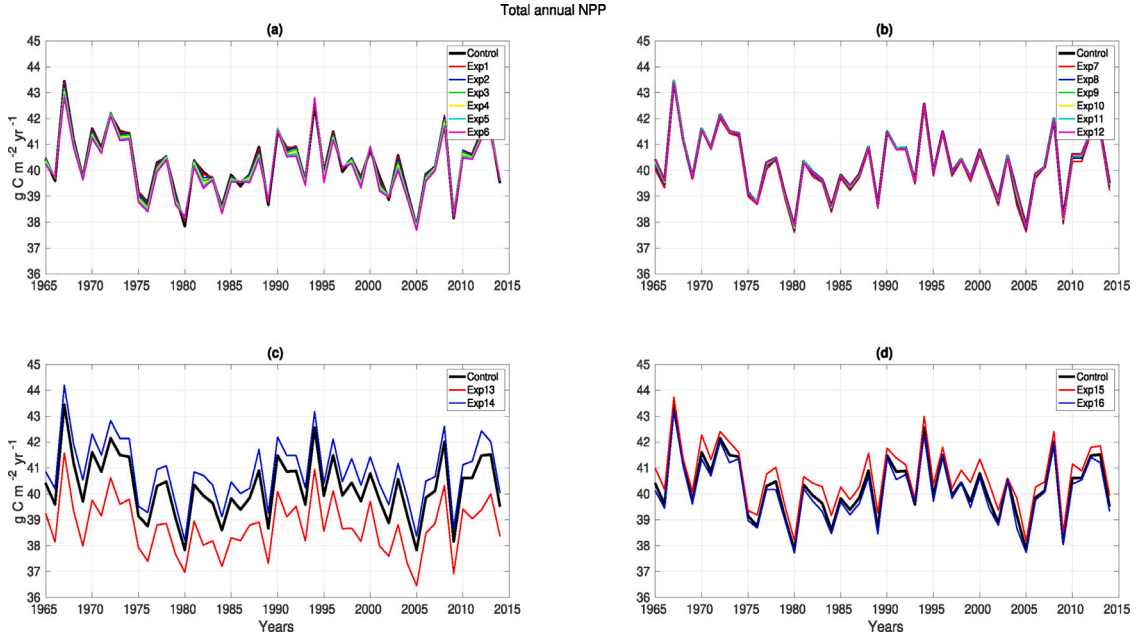

Fig. A.4. Depth-integrated total annual NPP from 1965 to 2015 for (a) Exps 1–6, (b) Exps 7–12, (c) Exps 13–14, and (d) Exps 15–16.

References

Alridge, J.N., Lessin, G., Amoudry, L.O., et al., 2017. Comparing benthic biogeochemistry at a sandy and a muddy site in the Celtic Sea using a model and observations. Biogeochemistry 135, 155–182.

Arhonditsis, G.B., Brett, M.T., 2004. Evaluation of the current state of mechanistic aquatic biogeochemical modeling. Mar. Ecol. Prog. Ser. 271, 13–26, https://www.int-res.com/abstracts/meps/v271/p13-26/.

Aumont, O., Ethé, C., Tagliabue, A., Bopp, L., Gehlen, M., 2015. PISCES-v2: an ocean biogeochemical model for carbon and ecosystem studies. Geosci. Model Dev. 8 (8), 2465–2513. http://dx.doi.org/10.5194/gmd-8-2465-2015, https://gmd.copernicus.org/articles/8/2465/2015/.

Bahamondes Dominguez, A.A., Hickman, A.E., Marsh, R., Moore, C.M., 2020. Constraining the response of phytoplankton to zooplankton grazing and photo-acclimation in a temperate shelf sea with a 1-D model – towards S2P3 v8.0. Geosci. Model Dev. 13 (9), 4019–4040. http://dx.doi.org/10.5194/gmd-13-4019-2020, https://gmd.copernicus.org/articles/13/4019/2020/.

Birchill, A.J., Hartner, N.T., Kunde, K., Siemering, B., Daniels, C., González-Santana, D., Milne, A., Ussher, S.J., Worsfold, P.J., Leopold, K., Painter, S.C., Lohan, M.C., 2019. The eastern extent of seasonal iron limitation in the high latitude North Atlantic Ocean. Sci. Rep. 9 (1), 1435. http://dx.doi.org/10.1038/s41598-018-37436-3.

Birchill, A.J., Milne, A., Woodward, E.M.S., Harris, C., Annett, A., Rusiecka, D., Achterberg, E.P., Gledhill, M., Ussher, S.J., Worsfold, P.J., Geibert, W., Lohan, M.C., 2017. Seasonal iron depletion in temperate shelf seas. Geophys. Res. Lett. 44 (17), 8987–8996. http://dx.doi.org/10.1002/2017GL073881, https://agupubs.onlinelibrary.wiley.com/doi/abs/10.1002/2017GL073881.

Bonnet, S., Guieu, C., Bruyant, F., Prášil, O., Van Wambeke, F., Raimbault, P., Moutin, T., Grob, C., Gorbunov, M.Y., Zehr, J.P., Masquelier, S.M., Garczarek, L., Claustre, H., 2008. Nutrient limitation of primary productivity in the Southeast Pacific (BIOSOPE cruise). Biogeosciences 5 (1), 215–225. http://dx.doi.org/10.5194/bg-5-215-2008, https://bg.copernicus.org/articles/5/215/2008/.

Boyd, P.W., Ellwood, M.J., 2010. The biogeochemical cycle of iron in the ocean. Nat. Geosci. 3 (10), 675–682. http://dx.doi.org/10.1038/ngeo964.

Boyd, P.W., Jickells, T., Law, C.S., Blain, S., Boyle, E.A., Buesseler, K.O., Coale, K.H., Cullen, J.J., de Baar, H.J.W., Follows, M., Harvey, M., Lancelot, C., Levasseur, M., Owens, N.P.J., Pollard, R., Rivkin, R.B., Sarmiento, J., Schoemann, V., Smetacek, V., Takeda, S., Tsuda, A., Turner, S., Watson, A.J., 2007. Mesoscale iron enrichment experiments 1993–2005: Synthesis and future directions. Science 315 (5812), 612–617. http://dx.doi.org/10.1126/science.1131669, https://www.science.org/doi/abs/10.1126/science.1131669.

Brewin, R.J., Tilstone, G.H., Jackson, T., Cain, T., Miller, P.I., Lange, P.K., Misra, A., Airs, R.L., 2017. Modelling size-fractionated primary production in the atlantic ocean from remote sensing. Prog. Oceanogr. 158, 130–149. http://dx.doi.org/10.1016/j.pocean.2017.02.002, https://www.sciencedirect.com/science/article/pii/S0079661116300350, The Atlantic Meridional Transect programme (1995-2016).

Browning, T.J., Liu, X., Zhang, R., Wen, Z., Liu, J., Zhou, Y., Xu, F., Cai, Y., Zhou, K., Cao, Z., Zhu, Y., Shi, D., Achterberg, E.P., Dai, M., 2022. Nutrient co-limitation in the subtropical Northwest Pacific. Limnol. Oceanogr. Lett. 7 (1), 52–61. http://dx.doi.org/10.1002/lol2.10205.

Buitenhuis, E., Le Quéré, C., Aumont, O., Beaugrand, G., Bunker, A., Hirst, A., Ikeda, T., O'Brien, T., Piontkovski, S., Straile, D., 2006. Biogeochemical fluxes through mesozooplankton. Glob. Biogeochem. Cycles 20 (2), http://dx.doi.org/10.1029/2005GB002511, https://agupubs.onlinelibrary.wiley.com/doi/abs/10.1029/2005GB002511.

Chase, Z., Hales, B., Cowles, T., Schwartz, R., van Geen, A., 2005. Distribution and variability of iron input to Oregon coastal waters during the upwelling season. J. Geophys. Res. Oceans 110 (C10), http://dx.doi.org/10.1029/2004JC002590, https://agupubs.onlinelibrary.wiley.com/doi/abs/10.1029/2004JC002590.

Conway, T.M., John, S.G., 2014. Quantification of dissolved iron sources to the North Atlantic Ocean. Nature 511 (7508), 212–215. http://dx.doi.org/10.1038/nature13482.

Curran, K., Brewin, R.J.W., Tilstone, G.H., Bouman, H.A., Hickman, A., 2018. Estimation of size-fractionated primary production from satellite ocean colour in UK Shelf Seas. Remote Sens. 10 (9), http://dx.doi.org/10.3390/rs10091389, https://www.mdpi.com/2072-4292/10/9/1389.

Dale, A.W., Nickelsen, L., Scholz, F., Hensen, C., Oschlies, A., Wallmann, K., 2015. A revised global estimate of dissolved iron fluxes from marine sediments. Glob. Biogeochem. Cycles 29 (5), 691–707. http://dx.doi.org/10.1002/2014GB005017, https://agupubs.onlinelibrary.wiley.com/doi/abs/10.1002/2014GB005017.

Davis, C., Mahaffey, C., Wolff, G., Sharples, J., 2014. A storm in a shelf sea: Variation in phosphorus distribution and organic matter stoichiometry. Geophys. Res. Lett. 41, http://dx.doi.org/10.1002/2014GL061949.

Dehairs, F., Baeyens, W., Van Gansbeke, D., 1989. Tight coupling between enrichment of iron and manganese in north sea suspended matter and sedimentary redox processes: Evidence for seasonal variability. Estuar. Coast. Shelf Sci. 29 (5), 457–471. http://dx.doi.org/10.1016/0272-7714(89)90080-2, https://www.sciencedirect.com/science/article/pii/0272771489900802.

Denman, K., Peña, M., 1999. A coupled 1-D biological/physical model of the northeast subarctic Pacific Ocean with iron limitation. Deep Sea Res. II 46 (11), 2877–2908. http://dx.doi.org/10.1016/S0967-0645(99)00087-9, https://www.sciencedirect.com/science/article/pii/S0967064599000879.

Dugdale, R.C., Goering, J.J., 1967. Uptake of new and regenerated forms of nitrogen in primary productivity. Limnol. Oceanogr. 12 (2), 196–206. http://dx.doi.org/10.4319/lo.1967.12.2.0196, https://aslopubs.onlinelibrary.wiley.com/doi/abs/10.4319/lo.1967.12.2.0196.

Edwards, A.M., 2001. Adding detritus to a nutrient–phytoplankton–zooplankton model:A dynamical-systems approach. J. Plankton Res. 23 (4), 389–413. http://dx.doi.org/10.1093/plankt/23.4.389.

Elrod, V.A., Berelson, W.M., Coale, K.H., Johnson, K.S., 2004. The flux of iron from continental shelf sediments: A missing source for global budgets. Geophys. Res. Lett. 31 (12), http://dx.doi.org/10.1029/2004GL020216, https://agupubs.onlinelibrary.wiley.com/doi/abs/10.1029/2004GL020216.

Elrod, V.A., Johnson, K.S., Fitzwater, S.E., Plant, J.N., 2008. A long-term, high-resolution record of surface water iron concentrations in the upwelling-driven central California region. J. Geophys. Res. Oceans 113 (C11), http://dx.doi.org/10.1029/2007JC004610, https://agupubs.onlinelibrary.wiley.com/doi/abs/10.1029/2007JC004610.

Eslinger, D.L., Iverson, R.L., 2001. The effects of convective and wind-driven mixing on spring phytoplankton dynamics in the Southeastern Bering Sea middle shelf domain. Cont. Shelf Res. 21 (6), 627–650. http://dx.doi.org/10.1016/S0278-4343(00)00106-0, https://www.sciencedirect.com/science/article/pii/S0278434300001060.

Everett, J.D., Baird, M.E., Buchanan, P., Bulman, C., Davies, C., Downie, R., Griffiths, C., Heneghan, R., Kloser, R.J., Laiolo, L., Lara-Lopez, A., Lozano-Montes, H., Matear, R.J., McEnnulty, F., Robson, B., Rochester, W., Skerratt, J., Smith, J.A., Strzelecki, J., Suthers, I.M., Swadling, K.M., van Ruth, P., Richardson, A.J., 2017. Modeling what we sample and sampling what we model: Challenges for zooplankton model assessment. Front. Mar. Sci. 4, http://dx.doi.org/10.3389/fmars.2017.00077, https://www.frontiersin.org/articles/10.3389/fmars.2017.00077.

Falkowski, P.G., 1997. Evolution of the nitrogen cycle and its influence on the biological sequestration of CO2 in the ocean. Nature 387 (6630), 272–275. http://dx.doi.org/10.1038/387272a0.

Fasham, M.J.R., Holligan, P.M., Pugh, P.R., 1983. The spatial and temporal development of the spring phytoplankton bloom in the Celtic Sea, April 1979. Prog. Oceanogr. 12, 87–145.

Fennel, W., 1995. A model of the yearly cycle of nutrients and plankton in the Baltic Sea. J. Mar. Syst. 6 (4), 313–329. http://dx.doi.org/10.1016/0924-7963(94)00031-6, https://www.sciencedirect.com/science/article/pii/0924796394000316.

Fiechter, J., Moore, A.M., Edwards, C.A., Bruland, K.W., Di Lorenzo, E., Lewis, C.V., Powell, T.M., Curchitser, E.N., Hedstrom, K., 2009. Modeling iron limitation of primary production in the coastal Gulf of Alaska. Deep Sea Res. II 56 (24), 2503–2519. http://dx.doi.org/10.1016/j.dsr2.2009.02.010, https://www.sciencedirect.com/science/article/pii/S0967064509000502, Physical and Biological Patterns, Processes, and Variability in the Northeast Pacific.

Floor, G.H., Clough, R., Lohan, M.C., Ussher, S.J., Worsfold, P.J., Quétel, C.R., 2015. Combined uncertainty estimation for the determination of the dissolved iron amount content in seawater using flow injection with chemiluminescence detection. Limnol. Oceanogr.: Methods 13 (12), 673–686. http://dx.doi.org/10.1002/lom3.10057, https://aslopubs.onlinelibrary.wiley.com/doi/abs/10.1002/lom3.10057.

Flynn, K.J., 2005. Castles built on sand: dysfunctionality in plankton models and the inadequacy of dialogue between biologists and modellers. J. Plankton Res. 27 (12), 1205–1210. http://dx.doi.org/10.1093/plankt/fbi099.

Flynn, K.J., 2010. Ecological modelling in a sea of variable stoichiometry: Dysfunctionality and the legacy of Redfield and Monod. Prog. Oceanogr. 84 (1), 52–65. http://dx.doi.org/10.1016/j.pocean.2009.09.006, https://www.sciencedirect.com/science/article/pii/S0079661109001396, Special Issue: Parameterisation of Trophic Interactions in Ecosystem Modelling.

Franks, P.J.S., 2002. NPZ models of plankton dynamics: Their construction, coupling to physics, and application. J. Oceanogr. 58 (2), 379–387. http://dx.doi.org/10.1023/A:1015874028196.

Geider, R.J., 1987. Light and temperature dependence of the carbon to chlorophyll-a ratio in microalgae and cyanobacteria: implications for physiology and growth of phytoplankton. New Phytol. 106 (1), 1–34. http://dx.doi.org/10.1111/j.1469-8137.1987.tb04788.x, https://nph.onlinelibrary.wiley.com/doi/abs/10.1111/j.1469-8137.1987.tb04788.x.

Geider, R.J., MacIntyre, H.L., Kana, T.M., 1998. A dynamic regulatory model of phytoplanktonic acclimation to light, nutrients, and temperature. Limnol. Oceanogr. 43 (4), 679–694. http://dx.doi.org/10.4319/lo.1998.43.4.0679.

Giering, S.L., Wells, S.R., Mayers, K.M., Schuster, H., Cornwell, L., Fileman, E.S., Atkinson, A., Cook, K.B., Preece, C., Mayor, D.J., 2018. Seasonal variation of zooplankton community structure and trophic position in the Celtic Sea: A stable isotope and biovolume spectrum approach. Prog. Oceanogr. 177, 101943. http://dx.doi.org/10.1016/j.pocean.2018.03.012, http://www.sciencedirect.com/science/article/pii/S0079661118300399, Shelf Sea Biogeochemistry: Pelagic Processes.

Hannon, E., Boyd, P., Silvoso, M., Lancelot, C., 2001. Modeling the bloom evolution and carbon flows during SOIREE: Implications for future in situ iron-enrichments in the Southern Ocean. Deep Sea Res. II 48 (11), 2745–2773. http://dx.doi.org/10.1016/S0967-0645(01)00016-9, https://www.sciencedirect.com/science/article/pii/S0967064501000169, The Southern Ocean Iron Release Experiment (SOIREE).

Hasumi, H., Nagata, T., 2014. Modeling the global cycle of marine dissolved organic matter and its influence on marine productivity. Ecol. Model. 288, 9–24. http://dx.doi.org/10.1016/j.ecolmodel.2014.05.009, https://www.sciencedirect.com/science/article/pii/S0304380014002580.

Heath, M.R., Beare, D.J., 2008. New primary production in northwest European shelf seas, 1960–2003. Mar. Ecol. Prog. Ser. 363, 183–203. http://dx.doi.org/10.3354/meps07460.

Hickman, A., Holligan, P., Moore, M., Sharples, J., Krivtsov, V., Palmer, M., 2009. Distribution and chromatic adaptation of phytoplankton within a shelf sea thermocline. Limnol. Oceanogr. 54, 525–536. http://dx.doi.org/10.4319/lo.2009.54.2.0525.

Hickman, A., Moore, M., Sharples, J., Lucas, M., Tilstone, G., Krivtsov, V., Holligan, P., 2012. Primary production and nitrate uptake within the seasonal thermocline of a stratified shelf sea. Mar. Ecol.-Prog. Ser. 463, 39–57. http://dx.doi.org/10.3354/meps09836.

Holligan, P.M., Williams, P.J., Purdie, D., Harris, D.S., 1984. Photosynthesis, respiration and nitrogen supply of plankton populations in stratified, frontal and tidally mixed shelf waters. Mar. Ecol. Prog. Ser. 17, 201–213.

Holt, J., Proctor, R., 2008. The seasonal circulation and volume transport on the northwest European continental shelf: A fine-resolution model study. J. Geophys. Res.: Oceans 113 (C6), http://dx.doi.org/10.1029/2006JC004034, https://agupubs.onlinelibrary.wiley.com/doi/abs/10.1029/2006JC004034.

Holt, J., Wakelin, S., Huthnance, J., 2009. Downwelling circulation of the northwest European continental shelf: A driving mechanism for the continental shelf carbon pump. Geophys. Res. Lett. 36, http://dx.doi.org/10.1029/2009GL038997.

Holt, J., Wakelin, S., Lowe, J., Tinker, J., 2010. The potential impacts of climate change on the hydrography of the northwest European continental shelf. Prog. Oceanogr. 86 (3), 361–379. http://dx.doi.org/10.1016/j.pocean.2010.05.003, https://www.sciencedirect.com/science/article/pii/S0079661110000856.

Homoky, W.B., Severmann, S., McManus, J., Berelson, W.M., Riedel, T.E., Statham, P.J., Mills, R.A., 2012. Dissolved oxygen and suspended particles regulate the benthic flux of iron from continental margins. Mar. Chem. 134–135, 59–70. http://dx.doi.org/10.1016/j.marchem.2012.03.003, https://www.sciencedirect.com/science/article/pii/S0304420312000424.

Hutchins, D.A., Bruland, K.W., 1998. Iron-limited diatom growth and Si:N uptake ratios in a coastal upwelling regime. Nature 393 (6685), 561–564. http://dx.doi.org/10.1038/31203.

Johnson, K.S., Chavez, F.P., Friederich, G.E., 1999. Continental-shelf sediment as a primary source of iron for coastal phytoplankton. Nature 398 (6729), 697–700. http://dx.doi.org/10.1038/19511.

Johnson, K.S., Gordon, R.M., Coale, K.H., 1997. What controls dissolved iron concentrations in the world ocean? Mar. Chem. 57 (3), 137–161. http://dx.doi.org/10.1016/S0304-4203(97)00043-1, https://www.sciencedirect.com/science/article/pii/S0304420397000431.

Joint, I.R., Owens, N.J.P., Pomroy, A.J., Pomeroy, A.J., 1986. Seasonal production of photosynthetic picoplankton and nanoplankton in the Celtic Sea. Mar. Ecol. Prog. Ser. 28 (3), 251–258, http://www.jstor.org/stable/24817442.

Joint, I.R., Pomroy, A.J., 1983. Production of picoplankton and small nanoplankton in the Celtic Sea. Mar. Biol. 77, 19–27.

Kanda, J., Ziemann, D.A., Conquest, L.D., Bienfang, P.K., 1989. Light-dependency of nitrate uptake by phytoplankton over the spring bloom in Auke Bay, Alaska. Mar. Biol. 103 (4), 563–569. http://dx.doi.org/10.1007/BF00399589.

Kaufman, D.E., Friedrichs, M.A.M., Smith Jr., W.O., Hofmann, E.E., Dinniman, M.S., Hemmings, J.C.P., 2017. Climate change impacts on southern Ross Sea phytoplankton composition, productivity, and export. J. Geophys. Res. Oceans 122 (3), 2339–2359. http://dx.doi.org/10.1002/2016JC012514, https://agupubs.onlinelibrary.wiley.com/doi/abs/10.1002/2016JC012514.

King, A.L., Barbeau, K., 2007. Evidence for phytoplankton iron limitation in the southern California Current System. Mar. Ecol. Prog. Ser. 342, 91–103, https://www.int-res.com/abstracts/meps/v342/p91-103/.

Kriest, I., Khatiwala, S., Oschlies, A., 2010. Towards an assessment of simple global marine biogeochemical models of different complexity. Prog. Oceanogr. 86 (3), 337–360. http://dx.doi.org/10.1016/j.pocean.2010.05.002, https://www.sciencedirect.com/science/article/pii/S0079661110000844.

Landry, M.R., Constantinou, J., Latasa, M., Brown, S.L., Bidigare, R.R., Ondrusek, M.E., 2000. Biological response to iron fertilization in the eastern equatorial Pacific (IronEx II). III. Dynamics of phytoplankton growth and microzooplankton grazing. Mar. Ecol. Prog. Ser. 201, 57–72, https://www.int-res.com/abstracts/meps/v201/p57-72/.

Li, Q., Legendre, L., Jiao, N., 2015. Phytoplankton responses to nitrogen and iron limitation in the tropical and subtropical Pacific Ocean. J. Plankton Res. 37 (2), 306–319. http://dx.doi.org/10.1093/plankt/fbv008.

Lis, H., Shaked, Y., Kranzler, C., Keren, N., Morel, F.M.M., 2015. Iron bioavailability to phytoplankton: an empirical approach. ISME J. 9 (4), 1003–1013. http://dx.doi.org/10.1038/ismej.2014.199.

Liu, K.-K., Yung Tang, T., Gong, G.-C., Chen, L.-Y., Shiah, F.-K., 2000. Cross-shelf and along-shelf nutrient fluxes derived from flow fields and chemical hydrography observed in the southern East China Sea off northern Taiwan. Cont. Shelf Res. 20 (4), 493–523. http://dx.doi.org/10.1016/S0278-4343(99)00083-7, https://www.sciencedirect.com/science/article/pii/S0278434399000837.

Lohan, M.C., Bruland, K.W., 2008. Elevated Fe(II) and dissolved fe in hypoxic shelf waters off oregon and washington: An enhanced source of iron to coastal upwelling regimes. Environ. Sci. Technol. 42 (17), 6462–6468. http://dx.doi.org/10.1021/es800144j.

Macdonald, H.S., Baird, M.E., Middleton, J.H., 2009. Effect of wind on continental shelf carbon fluxes off southeast Australia: A numerical model. J. Geophys. Res. Oceans 114 (C5), http://dx.doi.org/10.1029/2008JC004946, https://agupubs.onlinelibrary.wiley.com/doi/abs/10.1029/2008JC004946.

Maranon, E., Cermeno, P., Perez, V., 2005. Continuity in the photosynthetic production of dissolved organic carbon from eutrophic to oligotrophic waters. Mar. Ecol. Prog. Ser. 299, 7–17, https://www.int-res.com/abstracts/meps/v299/p7-17/.

Marsh, R., Hickman, A.E., Sharples, J., 2015. S2P3-R (v1.0): a framework for efficient regional modelling of physical and biological structures and processes in shelf seas. Geosci. Model Dev. Discuss. 8 (1), 673–713. http://dx.doi.org/10.5194/gmdd-8-673-2015.

Martin, J.H., Gordon, M., Fitzwater, S.E., 1991. The case for iron. Limnol. Oceanogr. 36 (8), 1793–1802. http://dx.doi.org/10.4319/lo.1991.36.8.1793, https://aslopubs.onlinelibrary.wiley.com/doi/abs/10.4319/lo.1991.36.8.1793.

Mills, M.M., Brown, Z.W., Laney, S.R., Ortega-Retuerta, E., Lowry, K.E., van Dijken, G.L., Arrigo, K.R., 2018. Nitrogen limitation of the summer phytoplankton and heterotrophic prokaryote communities in the Chukchi Sea. Front. Mar. Sci. 5, http://dx.doi.org/10.3389/fmars.2018.00362, https://www.frontiersin.org/articles/10.3389/fmars.2018.00362.

Mills, D., Laane, R., Rees, J., van der Loeff, M.R., Suylen, J., Pearce, D., Sivyer, D., Heins, C., Platt, K., Rawlinson, M., 2003. Smartbuoy: A marine environmental monitoring buoy with a difference. In: Dahlin, H., Flemming, N., Nittis, K., Petersson, S. (Eds.), Building the European Capacity in Operational Oceanography. In: Elsevier Oceanography Series, vol. 69, Elsevier, pp. 311–316. http://dx.doi.org/10.1016/S0422-9894(03)80050-8, http://www.sciencedirect.com/science/article/pii/S0422989403800508.

Moisander, P.H., Zhang, R., Boyle, E.A., Hewson, I., Montoya, J.P., Zehr, J.P., 2012. Analogous nutrient limitations in unicellular diazotrophs and Prochlorococcus in the South Pacific Ocean. ISME J. 6 (4), 733–744. http://dx.doi.org/10.1038/ismej.2011.152.

Moore, J., Doney, S.C., Glover, D.M., Fung, I.Y., 2001a. Iron cycling and nutrient-limitation patterns in surface waters of the World Ocean. Deep Sea Res. II 49 (1), 463–507. http://dx.doi.org/10.1016/S0967-0645(01)00109-6, https://www.sciencedirect.com/science/article/pii/S0967064501001096, The US JGOFS Synthesis and Modeling Project: Phase 1.

Moore, J., Doney, S.C., Kleypas, J.A., Glover, D.M., Fung, I.Y., 2001b. An intermediate complexity marine ecosystem model for the global domain. Deep Sea Res. II 49 (1), 403–462. http://dx.doi.org/10.1016/S0967-0645(01)00108-4, https://www.sciencedirect.com/science/article/pii/S0967064501001084, The US JGOFS Synthesis and Modeling Project: Phase 1.

Moore, C.M., Mills, M.M., Arrigo, K.R., Berman-Frank, I., Bopp, L., Boyd, P.W., Galbraith, E.D., Geider, R.J., Guieu, C., Jaccard, S.L., Jickells, T.D., La Roche, J., Lenton, T.M., Mahowald, N.M., Marañón, E., Marinov, I., Moore, J.K., Nakatsuka, T., Oschlies, A., Saito, M.A., Thingstad, T.F., Tsuda, A., Ulloa, O., 2013. Processes and patterns of oceanic nutrient limitation. Nat. Geosci. 6 (9), 701–710. http://dx.doi.org/10.1038/ngeo1765.

Moore, C.M., Mills, M.M., Langlois, R., Milne, A., Achterberg, E.P., La Roche, J., Geider, R.J., 2008. Relative influence of nitrogen and phosphorous availability on phytoplankton physiology and productivity in the oligotrophic sub-tropical North Atlantic Ocean. Limnol. Oceanogr. 53 (1), 291–305. http://dx.doi.org/10.4319/lo.2008.53.1.0291.

Moore, M., Suggett, D., Hickman, A., Kim, Y., Tweddle, J., Sharples, J., Geider, R., Holligan, P., 2006. Phytoplankton photoacclimation and photoadaptation in response to environmental gradients in a shelf sea. Limnol. Oceanogr. 51, 936–949. http://dx.doi.org/10.4319/lo.2006.51.2.0936.

Muller-Karger, F., Varela, R., Thunell, R., Luerssen, R., Hu, C., Walsh, J., 2005. The important of continental margins in the global carbon cycle. Geophys. Res. Lett. 32, http://dx.doi.org/10.1029/2004GL021346.

Nédélec, F., Statham, P.J., Mowlem, M., 2007. Processes influencing dissolved iron distributions below the surface at the Atlantic Ocean–Celtic Sea shelf edge. Mar. Chem. 104 (3), 156–170. http://dx.doi.org/10.1016/j.marchem.2006.10.011, https://www.sciencedirect.com/science/article/pii/S0304420306001861.

Obata, H., Karatani, H., Nakayama, E., 1993. Automated determination of iron in seawater by chelating resin concentration and chemiluminescence detection. Anal. Chem. 65 (11), 1524–1528. http://dx.doi.org/10.1021/ac00059a007.

Oliver, H., St-Laurent, P., Sherrell, R.M., Yager, P.L., 2019. Modeling iron and light controls on the summer phaeocystis antarctica bloom in the amundsen sea polynya. Glob. Biogeochem. Cycles 33 (5), 570–596. http://dx.doi.org/10.1029/2018GB006168, https://agupubs.onlinelibrary.wiley.com/doi/abs/10.1029/2018GB006168.

Öztürk, M., Croot, P.L., Bertilsson, S., Abrahamsson, K., Karlson, B., David, R., Fransson, A., Sakshaug, E., 2004. Iron enrichment and photoreduction of iron under UV and PAR in the presence of hydroxycarboxylic acid: implications for phytoplankton growth in the Southern Ocean. Deep Sea Res. II 51 (22), 2841–2856. http://dx.doi.org/10.1016/j.dsr2.2000.10.001, https://www.sciencedirect.com/science/article/pii/S0967064504001961, The SWEDARP 1997/98 Expedition.

Pingree, R.D., Holligan, P.M., Head, R.N., 1977. Survival of dinoflagellate blooms in the western English Channel. Nature 265 (5591), 266–269. http://dx.doi.org/10.1038/265266a0.

Pingree, R., Holligan, P., Mardell, G., 1978. The effects of vertical stability on phytoplankton distributions in the summer on the northwest European Shelf. Deep-Sea Res. 25 (11), 1011–1028. http://dx.doi.org/10.1016/0146-6291(78)90584-2, http://www.sciencedirect.com/science/article/pii/0146629178905842.

Pingree, R.D., Holligan, P.M., Mardell, G.T., Head, R.N., 1976. The influence of physical stability on spring, summer and autumn phytoplankton blooms in the Celtic Sea. J. Mar. Biol. Assoc. U. K. 56 (4), 845–873. http://dx.doi.org/10.1017/S0025315400020919.

Pingree, R.D., Pennycuick, L., 1975. Transfer of heat, fresh water and nutrients through the seasonal thermocline. J. Mar. Biol. Assoc. U. K. 55 (2), 261–274. http://dx.doi.org/10.1017/S0025315400015939.

Poulton, A.J., Davis, C.E., Daniels, C.J., Mayers, K.M., Harris, C., Tarran, G.A., Widdicombe, C.E., Woodward, E.M.S., 2019a. Seasonal phosphorus and carbon dynamics in a temperate shelf sea (Celtic Sea). Prog. Oceanogr. 177, 101872. http://dx.doi.org/10.1016/j.pocean.2017.11.001, https://www.sciencedirect.com/science/article/pii/S0079661117301581, Shelf Sea Biogeochemistry: Pelagic Processes.

Poulton, A.J., Mayers, K.M., Daniels, C.J., Stinchcombe, M.C., Woodward, E.M.S., Hopkins, J., Wihsgott, J.U., Widdicombe, C.E., 2019b. Dissolution dominates silica cycling in a shelf sea autumn bloom. Geophys. Res. Lett. 46 (12), 6765–6774. http://dx.doi.org/10.1029/2019GL083558, https://agupubs.onlinelibrary.wiley.com/doi/abs/10.1029/2019GL083558.

Powell, T.M., Lewis, C.V.W., Curchitser, E.N., Haidvogel, D.B., Hermann, A.J., Dobbins, E.L., 2006. Results from a three-dimensional, nested biological-physical model of the california current system and comparisons with statistics from satellite imagery. J. Geophys. Res. Oceans 111 (C7), http://dx.doi.org/10.1029/2004JC002506, https://agupubs.onlinelibrary.wiley.com/doi/abs/10.1029/2004JC002506.

Redfield, A.C., Ketchum, B.H., Richards, F.A., 1963. The influence of organisms on the composition of sea-water.

Rippeth, T.P., Palmer, M.R., Simpson, J.H., Fisher, N.R., Sharples, J., 2005. Thermocline mixing in summer stratified continental shelf seas. Geophys. Res. Lett. 32 (5), http://dx.doi.org/10.1029/2004GL022104, https://agupubs.onlinelibrary.wiley.com/doi/abs/10.1029/2004GL022104.

Rippeth, T.P., Wiles, P., Palmer, M.R., Sharples, J., Tweddle, J., 2009. The diapcynal nutrient flux and shear-induced diapcynal mixing in the seasonally stratified western Irish Sea. Cont. Shelf Res. 29 (13), 1580–1587. http://dx.doi.org/10.1016/j.csr.2009.04.009, https://www.sciencedirect.com/science/article/pii/S0278434309001605.

Roughan, M., Middleton, J.H., 2002. A comparison of observed upwelling mechanisms off the east coast of Australia. Cont. Shelf Res. 22 (17), 2551–2572. http://dx.doi.org/10.1016/S0278-4343(02)00101-2, https://www.sciencedirect.com/science/article/pii/S0278434302001012.

Ruiz-Castillo, E., Sharples, J., Hopkins, J., Woodward, M., 2019. Seasonality in the cross-shelf physical structure of a temperate shelf sea and the implications for nitrate supply. Prog. Oceanogr. 177, 101985. http://dx.doi.org/10.1016/j.pocean.2018.07.006, https://www.sciencedirect.com/science/article/pii/S0079661117302562, Shelf Sea Biogeochemistry: Pelagic Processes.

Santschi, P., Höhener, P., Benoit, G., Buchholtz-ten Brink, M., 1990. Chemical processes at the sediment-water interface. Mar. Chem. 30, 269–315. http://dx.doi.org/10.1016/0304-4203(90)90076-O, https://www.sciencedirect.com/science/article/pii/030442039090076O.

Sedwick, P.N., Blain, S., Quéguiner, B., Griffiths, F.B., Fiala, M., Bucciarelli, E., Denis, M., 2002. Resource limitation of phytoplankton growth in the Crozet Basin, Subantarctic Southern Ocean. Deep Sea Res. II 49 (16), 3327–3349. http://dx.doi.org/10.1016/S0967-0645(02)00086-3, https://www.sciencedirect.com/science/article/pii/S0967064502000863.

Severmann, S., McManus, J., Berelson, W.M., Hammond, D.E., 2010. The continental shelf benthic iron flux and its isotope composition. Geochim. Cosmochim. Acta 74 (14), 3984–4004. http://dx.doi.org/10.1016/j.gca.2010.04.022, https://www.sciencedirect.com/science/article/pii/S0016703710002073.

Sharples, J., 1999. Investigating the seasonal vertical structure of phytoplankton in shelf seas. Mar. Models 1 (1), 3–38. http://dx.doi.org/10.1016/S0079-6611(99)00002-6, http://www.sciencedirect.com/science/article/pii/S0079661199000026.

Sharples, J., 2008. Potential impacts of the spring-neap tidal cycle on shelf sea primary production. J. Plankton Res. 30, 183–197. http://dx.doi.org/10.1093/plankt/fbm088.

Sharples, J., Ellis, J.R., Nolan, G., Scott, B.E., 2013. Fishing and the oceanography of a stratified shelf sea. Prog. Oceanogr. 117, 130–139. http://dx.doi.org/10.1016/j.pocean.2013.06.014, https://www.sciencedirect.com/science/article/pii/S007966111300102X, From Physics to Fishing over a Shelf Sea Bank.

Sharples, J., Holligan, P.M., 2006. In: Robinson, A.R., Brink, K.H. (Eds.), Interdisciplinary Studies in the Celtic Seas, Vol. 14B. Harvard University Press, Boston, pp. 1003–1031.

Sharples, J., Moore, M.C., Rippeth, T.P., Holligan, P.M., Hydes, D.J., Fisher, N.R., Simpson, J.H., 2001. Phytoplankton distribution and survival in the thermocline. Limnol. Oceanogr. 46 (3), 486–496. http://dx.doi.org/10.4319/lo.2001.46.3.0486, https://aslopubs.onlinelibrary.wiley.com/doi/abs/10.4319/lo.2001.46.3.0486.

Sharples, J., Ross, O., Scott, B., Greenstreet, S., Fraser, H., 2006. Inter-annual variability in the timing of stratification and the spring bloom in the North-western North Sea. Cont. Shelf Res. 26, 733–751. http://dx.doi.org/10.1016/j.csr.2006.01.011.

Shropshire, T.A., Morey, S.L., Chassignet, E.P., Bozec, A., Coles, V.J., Landry, M.R., Swalethorp, R., Zapfe, G., Stukel, M.R., 2020. Quantifying spatiotemporal variability in zooplankton dynamics in the Gulf of Mexico with a physical–biogeochemical model. Biogeosciences 17 (13), 3385–3407. http://dx.doi.org/10.5194/bg-17-3385-2020, https://bg.copernicus.org/articles/17/3385/2020/.

Sigman, D.M., Boyle, E.A., 2000. Glacial/interglacial variations in atmospheric carbon dioxide. Nature 407 (6806), 859–869. http://dx.doi.org/10.1038/35038000.

Simpson, J.H., Sharples, J., 2012. Introduction to the Physical and Biological Oceanography of Shelf Seas. Cambridge University Press, http://dx.doi.org/10.1017/CBO9781139034098.

Smith, M.J., Tittensor, D.P., Lyutsarev, V., Murphy, E., 2015. Inferred support for disturbance-recovery hypothesis of North Atlantic phytoplankton blooms. J. Geophys. Res. Oceans 120 (10), 7067–7090. http://dx.doi.org/10.1002/2015JC011080, https://agupubs.onlinelibrary.wiley.com/doi/abs/10.1002/2015JC011080.

Steinacher, M., Joos, F., Frölicher, T.L., Bopp, L., Cadule, P., Cocco, V., Doney, S.C., Gehlen, M., Lindsay, K., Moore, J.K., Schneider, B., Segschneider, J., 2010. Projected 21st century decrease in marine productivity: a multi-model analysis. Biogeosciences 7 (3), 979–1005. http://dx.doi.org/10.5194/bg-7-979-2010, https://bg.copernicus.org/articles/7/979/2010/.

Steinberg, D.K., Landry, M.R., 2017. Zooplankton and the Ocean Carbon Cycle. Annu. Rev. Mar. Sci. 9 (1), 413–444. http://dx.doi.org/10.1146/annurev-marine-010814-015924, PMID: 27814033.

Sverdrup, H.U., 1953. On conditions for the vernal blooming of phytoplankton. ICES J. Mar. Sci. 18 (3), 287–295. http://dx.doi.org/10.1093/icesjms/18.3.287.

Taylor, A.H., Stephens, J.A., 1993. Diurnal variations of convective mixing and the spring bloom of phytoplankton. Deep Sea Res. II 40 (1), 389–408. http://dx.doi.org/10.1016/0967-0645(93)90023-G, https://www.sciencedirect.com/science/article/pii/096706459390023G.

Tsuda, A., Takeda, S., Saito, H., Nishioka, J., Nojiri, Y., Kudo, I., Kiyosawa, H., Shiomoto, A., Imai, K., Ono, T., Shimamoto, A., Tsumune, D., Yoshimura, T., Aono, T., Hinuma, A., Kinugasa, M., Suzuki, K., Sohrin, Y., Noiri, Y., Tani, H., Deguchi, Y., Tsurushima, N., Ogawa, H., Fukami, K., Kuma, K., Saino, T., 2003. A mesoscale iron enrichment in the western subarctic Pacific induces a large centric diatom bloom. Science 300 (5621), 958–961. http://dx.doi.org/10.1126/science.1082000, https://www.science.org/doi/abs/10.1126/science.1082000.

Turner, J.T., 2015. Zooplankton fecal pellets, marine snow, phytodetritus and the ocean's biological pump. Prog. Oceanogr. 130, 205–248. http://dx.doi.org/10.1016/j.pocean.2014.08.005, https://www.sciencedirect.com/science/article/pii/S0079661114001281.

Ussher, S.J., Worsfold, P.J., Achterberg, E.P., Laës, A., Blain, S., Laan, P., de Baar, H.J.W., 2007. Distribution and redox speciation of dissolved iron on the European continental margin. Limnol. Oceanogr. 52 (6), 2530–2539. http://dx.doi.org/10.4319/lo.2007.52.6.2530, https://aslopubs.onlinelibrary.wiley.com/doi/abs/10.4319/lo.2007.52.6.2530.

Wakelin, S., Holt, J., Proctor, R., 2009. The influence of initial conditions and open boundary conditions on shelf circulation in a 3D ocean-shelf model of the North East Atlantic. Ocean Dynam. 59, 67–81. http://dx.doi.org/10.1007/s10236-008-0164-3.

Williams, C., Sharples, J., Green, M., Mahaffey, C., Rippeth, T., 2013a. The maintenance of the subsurface chlorophyll maximum in the stratified western Irish Sea. Limnol. Oceanogr.: Fluids Environ. 3 (1), 61–73. http://dx.doi.org/10.1215/21573689-2285100, https://aslopubs.onlinelibrary.wiley.com/doi/abs/10.1215/21573689-2285100.

Williams, C., Sharples, J., Mahaffey, C., Rippeth, T., 2013b. Wind-driven nutrient pulses to the subsurface chlorophyll maximum in seasonally stratified shelf seas. Geophys. Res. Lett. 40 (20), 5467–5472. http://dx.doi.org/10.1002/2013GL058171, https://agupubs.onlinelibrary.wiley.com/doi/abs/10.1002/2013GL058171.

Wollast, R., 1998. In: Brink, K.H., Robinson, A.R. (Eds.), Evaluation and Comparison of the Global Carbon Cycle in the Coastal Zone and in the Open Ocean. The Sea, pp. 213–251.

Worthen, D.L., Arrigo, K.R., 2003. A coupled ocean-ecosystem model of the ross sea. Part 1: Interannual variability of primary production and phytoplankton community structure. In: Biogeochemistry of the Ross Sea. American Geophysical Union (AGU), pp. 93–105. http://dx.doi.org/10.1029/078ARS06, https://agupubs.onlinelibrary.wiley.com/doi/abs/10.1029/078ARS06.

Yin, K., Harrison, P.J., Pond, S., Beamish, R.J., 1995. Entrainment of nitrate in the Fraser River Estuary and its biological implications. III. Effects of winds. Estuar. Coast. Shelf Sci. 40 (5), 545–558. http://dx.doi.org/10.1006/ecss.1995.0037, https://www.sciencedirect.com/science/article/pii/S0272771485700376.

Yool, A., Popova, E.E., Anderson, T.R., 2013. MEDUSA-2.0: an intermediate complexity biogeochemical model of the marine carbon cycle for climate change and ocean acidification studies. Geosci. Model Dev. 6 (5), 1767–1811. http://dx.doi.org/10.5194/gmd-6-1767-2013, https://gmd.copernicus.org/articles/6/1767/2013/.